

UNIVERSITY OF NAPLES FEDERICO II

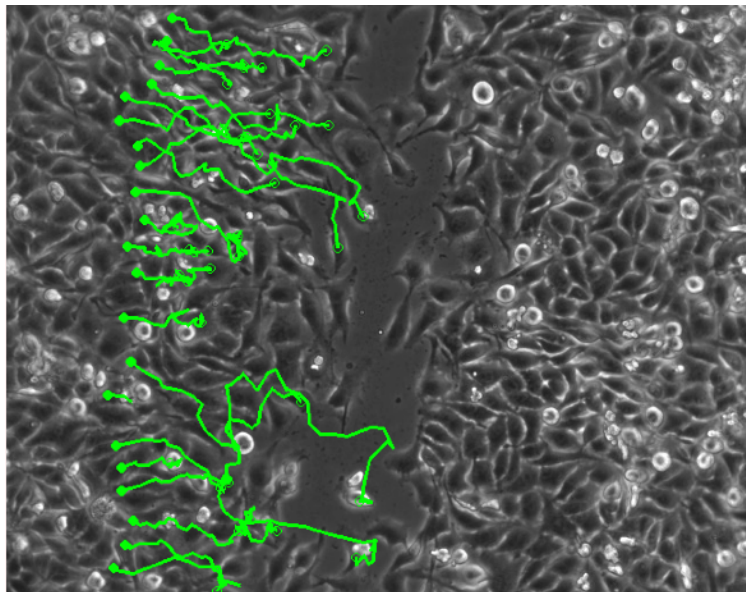
**DOCTORATE IN
MOLECULAR MEDICINE AND MEDICAL BIOTECHNOLOGY**

XXXII CYCLE



Rossella Tufano

**Evaluation of motility and proliferation of transformed cell lines by
computational analysis and in silico simulation**



Year 2020

UNIVERSITY OF NAPLES FEDERICO II

DOCTORATE IN
MOLECULAR MEDICINE AND MEDICAL BIOTECHNOLOGY

XXXII CYCLE



**Evaluation of motility and proliferation of transformed cell lines by
computational analysis and in silico simulation**

Tutor
Prof. Giovanni Paoletta

Candidate
Dr. Rossella Tufano

Coordinator
Prof. Vittorio Enrico Avvedimento

Year 2020

ABSTRACT	1
1. INTRODUCTION	2
1.1 Cell migration	2
1.1.1 Cell migration is involved in physiological and pathological processes	2
Immune response	2
Spreading of cancer cells	2
Wound healing	3
1.1.2 Mechanisms of cell migration, a multistep process	3
Cell polarization	3
Formation of protrusions	4
Adhesion to substrate	4
Cell body retraction and release of cell adhesions	5
Regulation by GTPases	5
Cell migration in 3D environments	6
1.2 Methods and tools used to study cell migration	6
1.2.1 Studying cell migration by time lapse microscopy	6
1.2.2 Image acquisition and cell tracking	7
1.2.3 Procedures for quantitative study of cell movement	9
Estimation of collective cell migration	9
Analysis of individual cell paths	10
1.2.4 Tools for movement analysis	11
1.3 MotoCell	12
2. AIM	13
3. MATERIALS AND METHODS	14
3.1 Cell propagation	14
3.2 Drugs	14
3.3 Microscopy and image acquisition	14
3.4 Mathematical models	15
3.5 Software development	16

3.5.1 Use of objects	16
3.5.2 PHP.....	16
3.5.3 R tool for statistical analysis	17
4. RESULTS.....	18
4.1 The main interface panels.....	18
Image display panel	19
Image collection panel.....	20
Movie collection panel	21
4.2 Management and simultaneous analysis of multiple time-lapse experiments	21
4.3 Quantitative analysis of cell movement	23
4.3.1 A family of analyzers	23
4.3.2 Data analysis in MotoCell.....	26
4.3.3 Data selection and functional reorganization	29
4.3.4 Modelling tools describing cell movement.....	32
4.4 Evaluation of cell proliferation and its effects	39
4.5 Simulation of synthetic cell populations	39
4.6 Motocell architecture.....	42
4.6.1 Objects hierarchy	43
4.6.2 Data objects.....	44
4.6.3 Interfacing with R	44
4.7 The analyser objects: MotoCell as a development environment.....	46
4.7.1 The analyzer objects.....	46
4.7.2 Services and functionalities available to analyser objects	47
5. CONCLUSIONS	51
6. ACKNOWLEDGEMENTS	53
7. REFERENCES.....	54
8. LIST OF PUBLICATIONS	65

ABSTRACT

Cell migration plays a crucial role in different pathological conditions, so a good understanding of the intra and extra cellular mechanisms involved could help in the development of new therapeutical strategies. Time-lapse microscopy is an excellent tool for dynamically studying cell movement. This work reports the development and testing of an integrated analysis environment based on MotoCell, a web application able to simultaneously manage time-lapse experiments, perform comparative analysis of multiple experiments extracting movement parameters, test models describing cell movement and proliferation and simulate the behaviour of cells growing on Petri dish via a simulation tool able to reproduce and predict the behaviour of cultured cells. The system includes additional tools that deal with acquisition and analysis of microscopy images and graphical representation of datasets containing cell paths obtained by tracking procedures.

1. INTRODUCTION

1.1 Cell migration

1.1.1 Cell migration is involved in physiological and pathological processes

Cell migration is a highly regulated process, involved in different physiological phenomena such as embryogenesis, organogenesis, wound repair and immune response. Abnormal regulation of this process is an important factor in the development of different pathological conditions including fibrosis, tumour invasion and atherosclerosis (for a review see Trepap et al., 2012).

Cells may move as independent entities or as a population, maintaining cohesive contacts and affecting one another while migrating.

Immune response

White blood cells (leukocytes) involved in immune response represent a good example of cells that prevalently move as single entities. During inflammatory response to a mechanical injury or to an infective process, circulating leukocytes are recruited from the bloodstream and move to the affected site (Muller, 2013). First of all, cells tether endothelial cells through adhesive molecules, expressed on the surface of both cell types; binding is greatly promoted by reduction of the blood flow at the inflammatory site. After that, cells roll along the endothelium and are further activated by chemokines and other pro-inflammatory molecules presented on them. Once activated, leukocytes become stuck to the endothelium by tight binding between integrin molecules in their membrane and ligands present on the surface of endothelial cells. In the end, they go across the endothelial cells, through an irreversible process defined diapedesis, traverse the interstitial tissue to finally reach the inflammation site.

Spreading of cancer cells

Another process in which single cell migration plays a crucial role is spreading of cancer cells or metastasis (Lambert et al., 2017; Dasgupta et al., 2017). Single cells detach from primary tumor, move towards and invade blood and lymphatic vessels, extracellular matrix and finally reach healthy tissue where they may develop a secondary tumor.

In recent years, the contribution of collective cell migration has emerged (Macpherson et al., 2007; Kawakami et al., 2009), supported by the presence of clusters of metastatic cells in patients with cancer and by the observation of chains, sheets and clusters of metastatic cells around the stroma areas of primary tumor in histopathological sections of breast, colon, ovarian, lung and other differentiated carcinomas. The relevant role of cell migration in this process

rather than proliferation and apoptosis is confirmed by results obtained by combining invasion assays with array-based gene expression analysis (Wang et al., 2005), which show that genes involved in pathways that regulate b-actin polymerization and cell protrusion are markedly upregulated. These results help explain the limited effect of killing invasive tumour cells by treatments that interfere with cell proliferation; drugs that block cell proliferation could still be used as a possible strategy to adopt in late phases to shrink secondary tumor (Chambers et al., 2002).

Wound healing

Cell movement is also involved in the healing of a skin wound, a complex process in which the contribute of several cell lineages and tissue is required. The skin with its epithelial (epidermis) and connective (derma) tissue layers is an important protective barrier against external agents, and if a break occurs, it has to be rapidly and efficiently repaired. In the beginning, blood leaked from damaged vessels produced by the wound sets to form a clot, which temporary protects the exposed tissues. Later on, fibroblasts and other inflammatory cells rush in to the clot, while epithelial cells at the wound edges start to proliferate and move, in order to fill the wounded area. The process requires about a week or two and may leave a scar; studies directed to investigate skin reconstruction are important to improve treatment of traumatic as well as surgical wounds (Martin, 1997; Wang et al., 2017).

1.1.2 Mechanisms of cell migration, a multistep process

Much knowledge about cell migration dynamics was acquired by observing and studying the behaviour of cultured fibroblasts on two-dimensional surfaces (Horwitz and Webb, 2003; Trepap et al., 2012). Fibroblasts move slower than other cell types such as keratinocytes and leukocytes, and the succession of different steps is more easily observed.

Cell polarization

After detecting a mechanical, chemical or other physical external stimuli, a fibroblasts polarize and define a leading and a rear edge. The leading edge will protrude towards the stimulus while the rear edge will retract. Fluorescence microscopy revealed that many signaling components are not uniformly distributed in polarized cells (Rappel and Edelstein Keshet, 2017); one of them is phosphatidylinositol (3,4,5)-triphosphate (PIP₃), whose level is higher at the leading than at the rear edge for the combined action of phosphoinositide-3 kinase (PI3K) and PTEN, a PIP₃ phosphatase. PIP₃ accumulation at the leading

edge recruits Rac and/or Cdc42, Rho family small guanosine triphosphatases (GTPases), that trigger downstream pathways leading actin polymerization.

Formation of protrusions

Actin filaments, while polymerizing, exert a force on the cell membrane and push it forward, forming protrusive structures such as broad lamellipodia or thin filopodia, characterized by different actin rearrangement and function. Lamellipodia are formed by a mesh of actin filaments and have an important role in defining the direction of cell migration, while filopodia are assembled as long parallel bundles beyond the lamellar edge and are supposed to be responsible for exploring environment during motility by functioning as chemical and mechanical sensors (Faix and Rottner, 2006; Gupton and Gertler, 2007; Kurosaka and Kashina, 2008; Ananthakrishnan and Ehrlicher, 2007). Different studies have suggested that inhibition of lamellipodia or filopodia formation does not inhibit cell movement, but affects speed and directionality of cells (Gupton et al., 2005; Yang and et al., 2007). Many of these aspects are observed both in single moving cells and in cells that collectively migrate as sheets (Horwitz and Webb, 2003; Mayor and Etienne-Manneville, 2016, De Pascalis and Etienne-Manneville, 2017).

Actin polymerization and depolymerization are dynamic processes, highly regulated by numerous proteins localized near or at the leading edge, such as WASP, a downstream target of Cdc42 and an activating protein that enables nucleator proteins such as actin-related protein (Arp)2/3 complex to initiate polymerization and assembly of actin modules that extend existing filaments. An additional regulator that can also take part in actin network growth is cofilin, an actin depolymerization promoting protein, that severs actin filaments and creates new plus ends for the growth of new actin filaments. Additional molecules that regulate actin dynamics are actin binding proteins, such as profilin and thymosine β -4, involved in maintaining a steady actin monomer pool for polymerization, cross linking and bundling proteins such as filamin, α -actinin, fascin, involved in formation of actin networks, capping proteins such as CapZ, that control filament length by capping actin filament ends and stopping polymerization and, severing and fragmenting proteins such as gelsolin and severin, that cut actin filaments and networks.

Adhesion to substrate

Once the protrusion at the leading edge has formed, it adheres to substratum by adhesion complexes. These attachment points connect actin cytoskeleton to the extracellular matrix, act as traction points and mediate intracellular signaling transduction that regulate adhesion dynamics and protrusive activity. In adhesion complexes catalytic and adaptor proteins have been identified. The

first group includes kinases, phosphatases, proteases and other enzymes such as phospholipase C- γ , while the second group includes proteins that mediate protein interactions by different protein-binding motifs such as LIM, calponin homology (CH), four point one ezrin radixin and moesin (FERM), PSD95/DlgA/ZO-1 homology (PDZ) domain, Src homology (SH) 2 and 3 domains. A key role in the assembly of adhesion complexes is played by integrins, heterodimeric proteins consisting of different combinations of α and β chains. After binding extracellular ligands, integrins change their conformation, clusterize by forming nascent adhesion structures called focal complexes that can mature into more stable and large focal adhesion and promote activation of intracellular pathways that involve Rho family of GTPase, ERK/MAP kinases and other regulatory molecules. Different studies have demonstrated that movement speed and adhesiveness are inversely proportional (Jurado et al. 2005). Adhesion to substrate have to be balanced, because weak adhesion structures are not sufficient to support traction, while with exceedingly strong ones movement is prevented.

Cell body retraction and release of cell adhesions

The last steps that allow cell movement are pulling of cell body towards the protrusion by contractile forces that are generated by the sliding of myosin motors on actin filaments and release of the adhesions in the rear edge, a myosin-mediated process. Both steps are regulated by Rho GTPases through effectors, such as ROCK, that regulate actomyosin contractility and release of adhesions; this last is also mediated by action of protease, calpain, which cleaves different focal adhesion proteins such as talin, vinculin (Horwitz and Webb, 2003; Ananthakrishnan and Ehrlicher, 2007; Wu, 2007).

Regulation by GTPases

The activity of GTPases controlling cell migration is regulated by the opposing actions of guanine nucleotide exchange factors (GEFs) and GTPase-activating proteins (GAPs). GEFs activate GTPases stimulating the exchange of a bound GDP nucleotide for GTP, while GAPs inactivate GTPases by catalyzing GTP hydrolysis. The role of GTPases has been known for over 20 years, but in recent years the high complexity of their regulation is emerged (Sadok and Marshall, 2014; Ridley, 2015; Haga and Ridley, 2016; Lawson and Ridley, 2018). RhoGEFs and RhoGAPs regulate many aspects involved in cell migration by forming complexes with other proteins. Most Rho GTPases are modified at their C-termini by isopropyl-lipids, which facilitate their localization to membranes. Rho guanine nucleotide dissociation inhibitors (GDIs) regulate RHOA, RAC1 and CDC42, by binding to isopropyl groups

and extracting them from membranes. GTPases are also regulated by other post translational modification such as phosphorylation and ubiquitylation.

Cell migration in 3D environments

Although, as mentioned above, most work directed to investigate cell movement dynamics has been performed in 2D cell culture, the behaviour of cells in 3D environments has also been studied. Migration patterns observed in 2D environments also occur in 3D tissue environments, but cell morphology is different in the two environments, because the distribution of ligands in 2D is typically more uniform than in 3D matrix. Typically in 3D matrices cells become elongated and perform more directional movements than those that migrate on 2D surfaces (Treat et al., 2012; Reig et al., 2014).

1.2 Methods and tools used to study cell migration

1.2.1 Studying cell migration by time lapse microscopy

Cellular movement is a dynamic process and largely benefits from continuous long-term observation of cell cultures, developing embryos and other experimental systems (Collins et al., 2018). Time-lapse microscopy is a powerful and continuously improving tool directed to investigate dynamic cellular processes and to observe the behaviour of cell populations as well as that of single cells within a population. It is performed by acquiring microscopy images at regular time intervals over an observation time that may vary from seconds to days according to the phenomenon in exam. Time-lapse microscopy was pioneered at the beginning of 20th century, but different improvements, mainly related to computer assisted image acquisition, made it an essential technique of studying dynamic phenomena such as cell division and death (Ortega et al., 2013; Yang et al., 2015; Kamlud et al., 2017; Dosch et al., 2018; Piltti et al., 2018), cell movement (Dai et al., 2005; Wagner et al., 2005; Wells and Ridley, 2005; Hossain et al., 2008; Arocena et al., 2010; Jain et al., 2012), evolution of cell-cell interactions (Merouane et al., 2015; Hirata et al., 2015; Ciccocioppo et al., 2015; Chen et al., 2016; Dosch et al., 2018), contact formation between cancer cells and environment (Al-toub et al., 2015), dynamics of subcellular organelles (Herman et al., 1984; Farnum et al., 1990). Time-lapse experiments have been an essential tool to study mammalian cells, but a great number of observations have also been carried out on prokaryotic and simpler unicellular or multicellular eukaryotic organisms (Kron et al., 2002; Kumar et al., 2016; Penil Cobo M. et al., 2018; Ungphakorn et al., 2017; Louvet et al., 2017; Ungphakorn et al., 2018; Schmidt et al., 2018).

Coutu and Schroeder (Coutu and Schroeder, 2013) pointed out the main problems related to long-term observations and possible solutions. During time-lapse experiments a critical point is to keep cells alive under the microscope stage over time and to recreate an environment as close as possible the one in which cells live. To this aim, an inverted microscope, equipped with a digital camera, is often associated with an incubator used to maintain, adjust and monitor CO₂, temperature, and humidity. CO₂ supply is important to maintain the physiological pH, but also to allow many cellular processes such as glucose metabolism and the correct function of ion and acid-base transporters. Phenol red, typically added to the culture medium to monitor pH changes, should be avoided if possible in fluorescence time-lapse microscopy, because of its fluorescence properties. A critical point is evaporation of the culture medium caused by constant gas exchange in the incubation chamber, which results in osmolarity changes of the medium by modifying the concentration of the solutes present in the medium; the effect is stronger for large incubators than cannot be fully humidified to prevent damage to oxidative-sensitive microscope parts. Evaporation can be prevented by using sealed chambers, covering medium with water-vapor-impermeable liquids such as mineral oil or using large volumes of medium, although this last strategy can produce increased noise in fluorescence images. More recently, time-lapse microscopy is emerging as a promising clinical technique (Collins et al., 2018), for example to select embryos for implantation (Sterckx et al. 2014, Sterckx et al. 2017), to assess *ex vivo* engineered cells for cell therapy (Schiraldi et al., 2014; Lin et al., 2014; Wei et al. 2015; Bago et al., 2016; Bago et al., 2016), to evaluate side effects of antibiotics (Turani et al., 2015) and efficacy of chemotherapeutics (Pulkkinen et al., 1996) or to estimate tumor malignancy (Weiger et al., 2013).

1.2.2 Image acquisition and cell tracking

During time lapse experiments, cells may be observed by bright field or phase contrast microscopy, as well as by taking advantage of fluorescence to highlight nuclei, membrane and other subcellular structures. Less frequently, confocal microscopy can be used to acquire z-axis stacks, used for detailed analysis of the whole cell volume. Confocal microscopy is expensive and generally more problematic as it increases the chances of phototoxic effects and is typically used only when three-dimensional information is absolutely required. To minimize phototoxicity, caused by short-wavelength light that reacts with cellular components or dyes and produce reactive oxygen species and free radicals that in turn damage DNA (Dixit and Cyr, 2003; Godley et al., 2005; Grzelak et al., 2001), one strategy is to reduce illumination. When samples are illuminated by visible light, acquisition can be recorded at high temporal resolution, but high energy short wave illumination should only be

used when necessary and for brief exposure times. Sometimes a combination of phase contrast and fluorescence microscopy, is used by taking, in addition to relatively rare fluorescence images or stacks, more frequent phase-contrast images, but these compromise approaches must be planned carefully and require instruments that can easily alternate fluorescent and bright-field microscopy (Baker, 2010).

Quantitative estimation of migration requires manual or automatic cell tracking procedures. Manual tracking is carried out by an operator who selects a reference point within a cell for each time-lapse frame. This approach is often accurate, but it is time-consuming and affected by the difficulty to univocally identify a reference point and by inconsistencies between different operators. For these reasons different automatic cell tracking algorithms have been proposed. Although their ability to track cells without errors is limited, these are often used especially when large number of cells and/or cultures need to be followed. Automatic cell tracking procedures may be classified in three main groups (Svensson et al., 2017): tracking by detection, tracking by model evolution and tracking by filtering. At the first group belong algorithms that separate the objects of interest, i.e. single cells or cell clusters, from background by a segmentation process. This separation may be obtained by using a single threshold value, chosen so that all image pixels that are above it are selected as ‘cells’, while the others are assigned to ‘background’, but this approach is not usable for samples that are not uniformly illuminated; in these cases local adaptive thresholding may be used to calculate a different threshold value for each pixel, chosen on the basis of the intensity values of neighbouring pixels. Other approaches to segment images use ‘edge detection’, i.e. a method which relies on the concept that close to an edge there is often a consistent change of intensity. Although this approach is more robust of the others mentioned above, it still fails too often for “difficult” images, such as low contrast ones.

Another limitation of these approaches is that they are not able at separating cells from each other with the same efficiency obtained in separating cells from the background; “watershed” filters have been used to identify local minimum levels to use as borders.

Algorithms in the second group consider each tracked object as a deformable model, whose margins are calculated in the first frame and then iteratively modified in time by minimising a specific energy function (Ray and Acton, 2002; Li et al., 2008; Yang et al., 2005, Dufour et al., 2005, Dzyubachyk et al., 2010). The procedures of the last group (Liu, 2008) are composed of three main steps that are performed iteratively. Starting from random particles with associated weights, during the selection phase the particles with the highest posterior probability are chosen among the previous particle set, then in the prediction step each particle is modified according to the state model, then in

the measurement step the weight of each particle is reassigned based on new data.

1.2.3 Procedures for quantitative study of cell movement

The results of time-lapse acquisitions and cell tracking procedures are both routinely analyzed to quantitatively estimate collective and/or single cell migration parameters.

Estimation of collective cell migration

Examples of collective cell migration analysis include aspects such as degree of plate coverage expressed as percent confluence or advancement of a cell front as in wound healing assay. Fig. 1.2.3.1 (A) shows a schematic representation of collective analysis used to determine wound size and

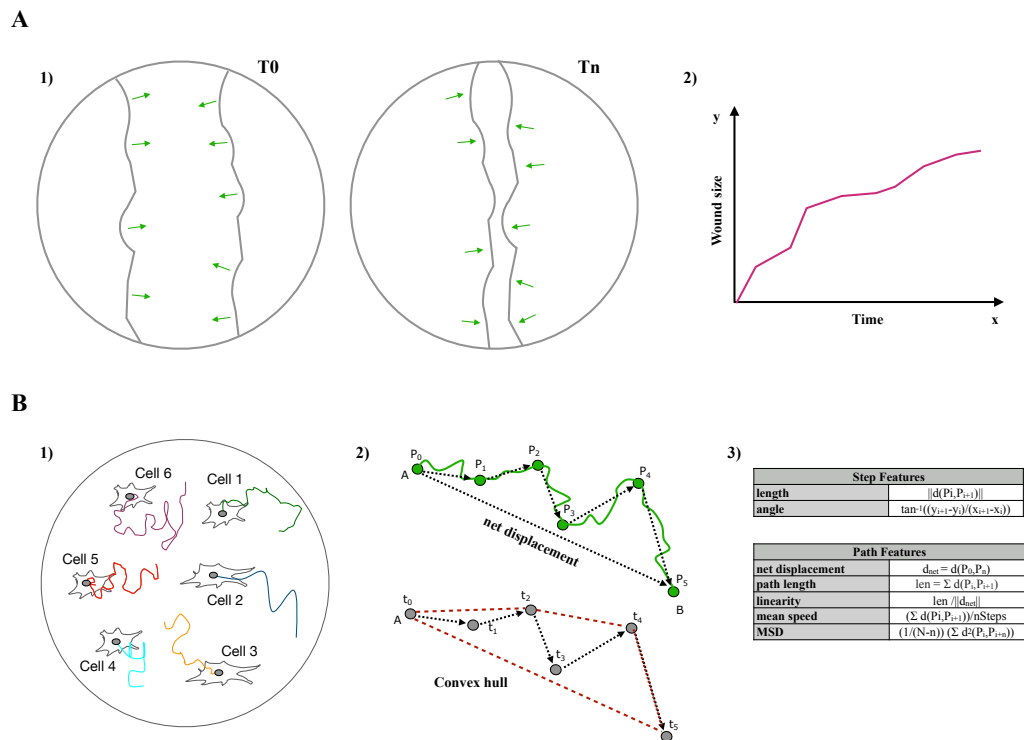


Figure 1.2.3.1 Quantitative study of cell movement (A) Wound closure rates are estimated by evaluating the advancement of a cell population front at a given time (middle), compared to the beginning of the experiment (left) and displayed as a function of time (right). (B) Single cell analysis is performed by determining trajectories of individual cells by tracking procedures (left). The acquired x-y coordinates at each time point (middle) are used to calculate descriptive parameters such as net displacement, distance between start and end point of a path (middle top), convex hull, i.e. the smallest set of points that contains the path (middle bottom), linearity, mean speed, MSD according to the formulas on the right.

migration rates: image segmentation or other methods are used to evaluate the

advancement of a cell population starting from a series of images contained in a time-lapse stack. Migration rates have been calculated as wound size difference between a given time point and the beginning of the observation, difference in the wound size between subsequent frames, percent changes in wound area, slope of the Richards function (a sigmoid function) that fit with temporal trend of the wound area (Liang et al., 2007; Büth et al., 2007; Walter et al. 2010; Ranzato et al., 2011; Topman et al. 2012). Coordinated movement in a cell layer, or in a specific area of the layer, was estimated by calculating the velocity correlation length (Petitjean et al., 2010; Milde et al., 2012).

Analysis of individual cell paths

To independently analyze single cell migration, the coordinates of each cell, acquired during the cell tracking phase, are used to calculate parameters that describe the displacement among two subsequent frames or total displacement of a cell (Fig. 1.2.3.1 B). Displacements are vectors, characterized by a length and a direction. Their length can be used to calculate mean speed, total distance traveled by a cell, net displacement i.e. the distance between start and end point, linearity, defined as the ratio between path length and net displacement. An arrest coefficient may be calculated, based on a threshold speed that the operator chooses to define that a cell is pausing, to indicate how many times a cell stays still. Additional information can be obtained by determining a convex hull, the smallest set of points that contains the tracked path, and calculating its perimeter, area and circularity (Debeir et al., 2008; Mokhtari et al., 2013).

Different migration models have been used to describe movement and to quantify differences between cells or populations. Movement expressed as mean squared displacement (MSD) as a function of time is used to describe diffusive movement of a cell (Codling et al., 2008), starting from the knowledge that the value of MSD of purely random moving entities is proportional to time, and that faster changes characterise superdiffusive movement, while a system that evolves more slowly is classified as subdiffusive. However, this measure does not uniquely describe migration, for example it has been shown that in lymph nodes, T cells with different movement types can produce similar MSD profiles (Beltman et al., 2009; Svensson et al., 2017).

The combination of wet lab experiments with *in silico* modelling has been shown to be extremely powerful for cell migration research (Rosello et al., 2004; Safferling et al. 2013), above all for tumor invasion studies (Sanga et al., 2007; Anderson et al., 2008; Kam et al., 2012). In *in silico* experiments, the evolution in time and space of a cell and its components is described by a set of mathematical equations. Cells can be represented as continuum models or agent-based models (ABM). In the first case cells are considered as a group

that shares the same properties, while in the second case each cell is a single entity that interacts with the others. The simulation of each single cell may be prohibitive, above all with a great number of cells, so this approach is preferred to simulate condition in which the number of cells is restrained. The ABMs models may be further divided into two groups, namely nuclei-centered and deformable models, on the basis of their representation in space. Indeed, while in the first group cells are represented by their nuclei, in the second one the cells are single entities with their own shape, volume or area that evolve in time on the basis of the cell state or of interactions with neighbouring cells and other environmental components.

1.2.4 Tools for movement analysis

Several tools, both commercial and available as free software, have been developed over the years to investigate intracellular and extracellular mechanisms involved in cell migration (for reviews see Masuzzo et al. 2016). Most of them have support for image processing, segmentation and cell tracking, but not many include advanced tools specific for quantitative analysis of cell migration.

Some tools were implemented as plug-ins of imageJ, for example Adapt (Barry et al., 2005), that detects cell trajectories as well as filopodia and blebs. While iTrack4U (Cordelières et al., 2013) is an automatic cell tracking program which use mean-shift algorithm and computes different variables that characterise cell trajectories and motility.

Specific tools have been developed to analyze collective cell migration such as AVeMap (Deforet et al., 2012), Cell Image Velocimetry (Milde et al., 2012), TScratch (Gebäck et al., 2009). Differences among these free tools include the algorithm adopted to segment cells and the parameters calculated to estimate collective cell migration. AVeMap performs a fully automated correlation-based method to segment cells, the parameters calculated are velocity, wound area, wound edge tortuosity, quality index. Cell Image Velocimetry carries out image velocimetry algorithms, that were found particularly effective to process images with low signal to noise ratio and/or contrast. TScratch uses the fast discrete curvelet transform to separate background from cells in the bright field images, then the open area, defined as the ratio between later time point measurement and initial measurement, is measured for each image and may be eventually manually modified. Other tools, such as CellProfiler (Carpenter et al., 2006) and Pathfinder (Chapnick et al., 2013), have been developed to estimate single-cell and collective migration. For each identified cell and sub-cellular compartment, CellProfiler calculates location, area, shape, Zernike shape features, Haralick and Gabor texture features. The tool is also able to measure other objects, such as yeast colonies, yeast growth patches, wounds in

scratch assays and tumors. In addition, thanks to its modular structure new algorithms may be added.

For each detected cell, Pathfinder, calculates from fluorescence microscopy images, speed and angle values, but also the changes of these parameters in time. In particular at each time point, the angle of deflection, defined as the angle between two lines, that are two consecutive displacements, is calculated. These data are used to estimate the migration persistence, measured as the average absolute angle of deflection: a decrease of this value reflects an increase of cell population persistence. The standard deviation of the distribution of all trajectory angles is also calculated: large values indicate that the cells are moving in different directions, without following a specific one. Pathfinder, unlike other tools that quantify collective migration, does not calculate wound size of the segmented area.

1.3 MotoCell

MotoCell (Cantarella et al. 2009) is a web application, previously developed in the hosting laboratory, directed to quantitatively study the motility of cell populations, maintained in different experimental conditions. The software was originally developed to track and analyze the paths covered by cultured cells on a surface during the observation time. MotoCell was designed to load an image stack acquired by time-lapse microscopy, and to record cell paths by clicking the positions of cells in subsequent frames and registering at the same time also cell origin and destiny (death, split after a mitotic event or move out of the observation field). Tracked paths may be displayed over the images, edited to correct eventual errors and stored into a text file; data stored in this file are analysed by calculating for each cell or for the whole population, movement parameters such as path length, average speed, linearity, average angle. Directional movement may be studied by circular statistics analysis by calculating linear dispersion coefficient (R) and angular dispersion coefficient (S) to detect the non-uniform distribution of angles, without discriminate between different non-uniform distributions; curve fitting to Von Mises and uniform circular distributions are used to assess whether movement is concentrated around a mean direction, as it happens in unidirectional movement. Watson test is also integrated to assess the goodness of fit. Additional tools allow to evaluate the behaviour of cells in time, so speed, persistence and mean angle are calculated by averaging the values at each time point.

2. AIM

The aim of this work was to evaluate cell movement in transformed cell lines by time lapse microscopy, computational analysis and *in silico* simulation, in order to investigate intra and extra cellular aspects involved in this phenomenon. Main goals were to create an environment in which comparative analysis of many time lapse experiments, modelling and simulation of eukaryotic cell cultures were all integrated.

3. MATERIALS AND METHODS

3.1 Cell propagation

Computational procedures projected and realized during this work have been used to study migration and proliferation of several cell lines, by comparing their behaviour in different experimental situations. NIH3T3 murine fibroblasts, NIH3T3 transformed murine fibroblast, HeLa cells from cervix adenocarcinoma, MDA-MB231 metastatic cells from pleural effusion of breast adenocarcinoma, PC3 from prostate adenocarcinoma, T24 from urinary bladder carcinoma, were cultured in 100mm diameter Petri plates, in growth medium prepared with DMEM (Dulbecco's Modified Eagle's Medium) and FBS (Fetal Bovine Serum) at appropriate concentrations and supplemented with penicillin (10 U/ml), streptomycin (10 ng/ml) and L-Glutamine (2mM). Cultures were maintained at 37°C and 5% CO₂ in a humidified incubator. For propagation and plating, cells were detached from the culture plate with Trypsin/EDTA (0.05%/0.53 mM), collected with culture medium and resuspended after centrifugation at 1200 rpm for 10 minutes. In order to seed cells at precise density in 12 well plates, a Burker chamber was used.

3.2 Drugs

FR180204 (5-(2-Phenyl-pyrazolo[1,5-a]pyridin-3-yl)-1H-pyrazolo[3,4-c]pyridazin-3-ylamine), is a competitive inhibitor of Erk1/Erk2 which interacts with nucleotide binding domain. Stock solution was prepared dissolving the inhibitor in DMSO at final concentration of 3 mM.

XMD8-92(2-[[2-Ethoxy-4-(4-hydroxy-1-piperidinyl)phenyl]amino]-5,11-dihydro-5,11-dimethyl-6H-pyrimido[4,5-b][1,4]benzodiazepin-6-one) is a competitive inhibitor of Erk5 for nucleotide binding domain. Stock solution was prepared dissolving the inhibitor in in DMSO at final concentration of 10 mM.

LY 294002 (2-(4-Morpholinyl)-8-phenyl-4H-1-benzopyran-4-one)) was purchased from Calbiochem. A stock solution (10 mM) was prepared in DMSO, stored at -20°C and used at final concentration of 10 μM.

3.3 Microscopy and image acquisition

For microscopic observations, cells were seeded in complete growth medium. Random migration experiments were done by plating cells at low density, while for wound-healing experiments, cells were grown to obtain confluent monolayers, then scratched with a tip. The classic wound-healing assay was used in combination with time-lapse microscopy to obtain live cell imaging. Image stacks have been acquired by using the experimental setup reported in fig. 3.3.1. The system is composed by an inverted microscope (Zeiss Axiovert



Figure 3.3.1 Experimental setup for time-lapse image acquisition.

200M) with motorized stage which allows to move the sample along three axes (x, y and z) and permits prolonged automatic acquisition at different positions or levels; an incubator chamber is used to maintain the conditions necessary for long time observations of living cells and a digital camera (AxioCam H/R) has been used to acquire digital images of the observation field. The microscope is connected to an Intel personal computer running Window XP, through the Zeiss acquisition software (Axiovision 6.0) that is used to manage the microscope and capture images. Within this work, digital frames were in most cases acquired with 10 minutes intervals for 24 hours or more.

3.4 Mathematical models

Curve fitting analyses performed in MotoCell rely on the *nls* (non-linear least squared) method available in R.

The proliferation analysis discussed under 4.4 has been performed by fitting Weibull distribution whose equation is reported here after:

$$y = Asym - (Asym - 1) \cdot e^{-e^{lrc \cdot x^{shape}}}$$

where *Asym* is the asymptote of the curve, *shape* is a parameter whose value is one for an exponential curve and larger as the distribution is more sigmoidal, *lrc* is a scale parameter that becomes bigger as the curve spreads out.

Movement modelling tools analyze the relationship between mean squared displacement (MSD) and time for an observation time whose amplitude can be decided by the users through a dialog box. The analyses are carried out on overlapping time windows to evaluate cell behaviour in time.

The diffusion analysis discussed under 4.3.3 has been carried out by fitting diffusive model to mean squared displacement (MSD) in time. Diffusive model function is:

$$MSD = kt^\alpha$$

where k is a coefficient that depends on cell velocity and α a value between 1 and 2, coming from diffusive to ballistic behaviour.

In the persistence analysis the same data are tested by using the persistent model function:

$$MSD = 2S^2P[t - P(1 - e^{-\frac{t}{P}})]$$

where S is the root mean squared speed and P is the directional persistence time. In these analyses, at each MSD calculated is assigned a different weight on the basis of how many squared displacements have been contributed to the calculation of the average.

The analysis tool that models MSDs as the sum of three components initially calculates the bias vector by performing the vectorial sum of all cell displacements. After this, for each displacement, its projection on the bias direction (d_b) and the difference between the previous step and the direction of the bias are calculated. The results are used to fit the following function:

$$d_b = b + p \cdot \cos(\alpha)$$

where bias (b) and persistence (p) vectors are quantified and then subtracted from each displacement to obtain the corresponding random vector (r).

3.5 Software development

3.5.1 Use of objects

MotoCell has been developed by using the object-oriented programming (OOP), by taking advantages of the ability to create modules that do not need changing when a new type of object is added. New objects are created by extension of existing objects and inherit all of their features. Each object's data and logic is essentially hidden from other objects. The OOP approach has been heavily used to develop modular software where different tools share the same objects and so acquire specific characteristics and behaviour.

3.5.2 PHP

PHP (website: PHP) is the main programming language used during the development of MotoCell. PHP is a scripting language, originally designed for producing dynamic web pages and it is tight integrate with the Apache server. Within MotoCell, PHP has been occasionally used as a simple scripting

language for web pages but mostly as a standard language for the development of complex multifile programs. The version currently in use is PHP 5.6.30.

3.5.3 R tool for statistical analysis

Within MotoCell, different analysis use R, an open source environment for statistical computing and graphics, which runs on a wide variety of platforms. R is a combination of different statistics packages and programming languages. In the R environment, there are several packages supplied for statistical techniques, which can be extended via packages available through the CRAN family. The software version used was R 3.3.2.

4. RESULTS

A major achievement of this work has been setting up an integrated analysis environment to study cell movement by computational analysis of cultured cell populations observed in time-lapse microscopy experiments. The environment is based on MotoCell, a web application previously developed in the hosting laboratory, which was completely reorganized and mostly rewritten to generate an extendable development environment where new tests and analysis procedures may be easily introduced. The “new” MotoCell includes tests for different movement models and is an effective tool for comparative analysis of multiple time-lapse experiments. It was complemented by interfacing with a simulation tool, used to predict the evolution of synthetic cell populations which reproduce the behaviour of experimental cell lines observed under specific conditions. A number of satellite tools were added to deal specific functionalities such as image acquisition and analysis, dynamic movie display and others. Within this environment it is possible to acquire, manage, analyze, model and simulate cell cultures grown on petri dishes or other supports and observed in time.

4.1 The main interface panels

MotoCell interface (figure 4.1.1) is organized in an application header, also used to customise the main settings of the application, such as units of measurement for lengths, angles and time, and a main area where most activities are carried out. This includes the image display panel, where cell paths are built, edited and visualized superimposed onto the acquired images and two panels used to respectively manage the collection of image stacks and

Title	Frames	Min	Duration	Cell line	Condition
sample_Hela_ch20	145	10	1440	-	-
stg_ch1_2j778a	145	10	1440	-	-
sample_Hela_ch20	145	10	1440	-	-

Title	Paths	Stack ID	Cell line	Condition
ch1-left	41	-	-	-
ch1-right	41	-	-	-
ch1-left	41	-	-	-
merge-ch1	82	-	-	-

ID	Start	Origin	End	Destiny	Mother ID
P1	0	start	144	end	-
P2	0	start	12	split	-
P3	12	split	144	end	P2
P4	12	split	144	end	P2
P5	0	start	88	split	-
P6	88	split	144	end	P5
P7	88	split	144	end	P5
P8	0	start	144	end	-
P9	0	start	68	split	-

Figure 4.1.1 MotoCell interface. The figure shows the main MotoCell interface window after loading three image stacks and four *movie* files. The second image stack is currently displayed in the left panel, together with the paths from the third *movie* file, which is also displayed in detail mode below the list of the loaded *movies*.

available to the application and the loaded datasets (*movies*), containing the paths followed by individually tracked cells.

Image display panel

The image display panel (fig. 4.1.2), is used to build, display and edit cell paths stored in *movie* files. In the new MotoCell the display panel is completely based on new, more powerful, *movie* object (see below under Architecture) used to read, convert and store *movies*, as well as to extract data according to specific filters. The new interface allows to keep many *movies* open at the same

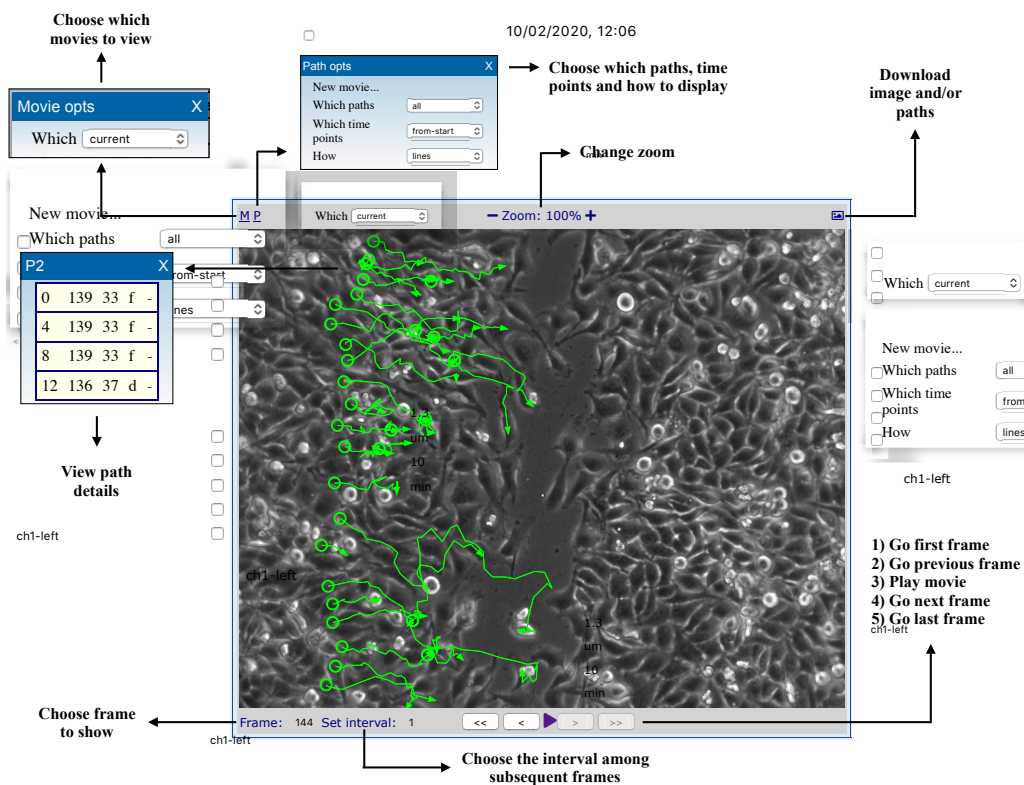


Figure 4.1.2 Organization of the image display panel. The figure shows the image display panel annotated with arrows pointing to the main functions. The palettes displayed around the main panel are used within the application to choose the *movie* file to be superimposed to the image (top left), the *paths* to display and how to draw them (top), to show the locations included in the selected path (left).

time, and to quickly switch from one to the other. The user interface is now much improved, as cell paths superimposed on the image can now be graphically selected by clicking on the path and edited by clicking and dragging the points representing the position of a cell at each time point. The panel is also used for selecting paths and/or areas of an image (see below).

Image collection panel

The image collection panel, shown in fig. 4.1.3, was introduced to add the capability to manage image stacks from many time-lapse experiments at the same time. *Movies* to be compared may in fact come from the same image stack, but more often derive from stacks corresponding to different experiments. The interface panel was designed to manage many image stacks at the same time, and movie-stack mapping was introduced, to enable MotoCell to work on different experiments, while correctly keeping each *movie* aligned with the corresponding image stack. The panel contains a table reporting the available stacks with essential details, such as ID, number of images, duration of acquisition and other experimental conditions.

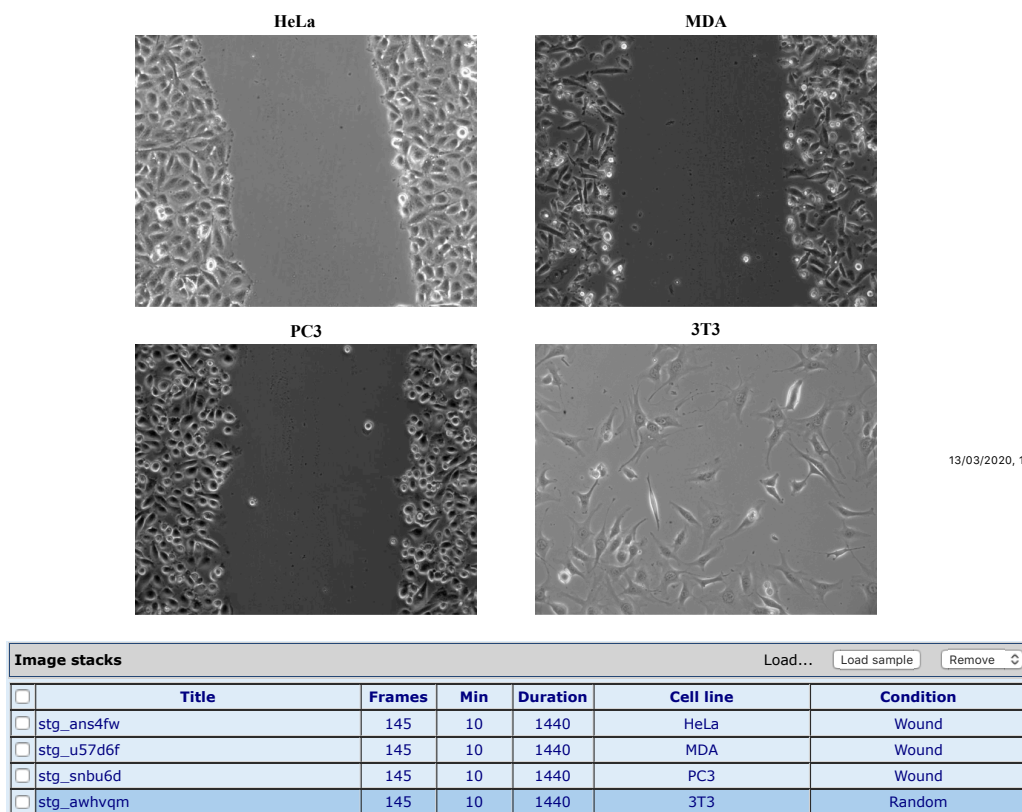


Figure 4.1.3 Multiple stacks displayed within the application interface. The figure shows the content of the image display panel while displaying a representative image from each of four image stacks obtained from time-lapse recording of different cell lines in culture (top) and the image collection interface panel used to display info about the stacks and to select them (bottom).

Movie collection panel

The *movie* collection panel, is used to manage datasets contained in *movie* files, i.e. text files containing the description of the experiment in terms of locations occupied by the observed cells, details of the culture conditions and events occurred during the observation time. It is organized in two sections, the upper one hosting a table of the currently loaded datasets, and the lower one containing the main features of the currently selected dataset. The panel is extensively used for management of multiple experiments and is better detailed in the next section.

4.2 Management and simultaneous analysis of multiple time-lapse experiments

Comparative analysis of different experiments is necessary to identify similarities and highlight differences among them. To effectively compare the behaviour of cell populations within MotoCell, a major rewriting of the input and analysis sections was undertaken, within which the application was substantially modified to add the ability to upload and manage groups of coordinate files at the same time and to carry out comparative analysis. Specifically, a dedicated tool, whose functions are accessible through the *movie* collection panel (fig. 4.2.1), was built to manage different datasets contained in coordinate files, that in our system are called *movies*. For each dataset, the

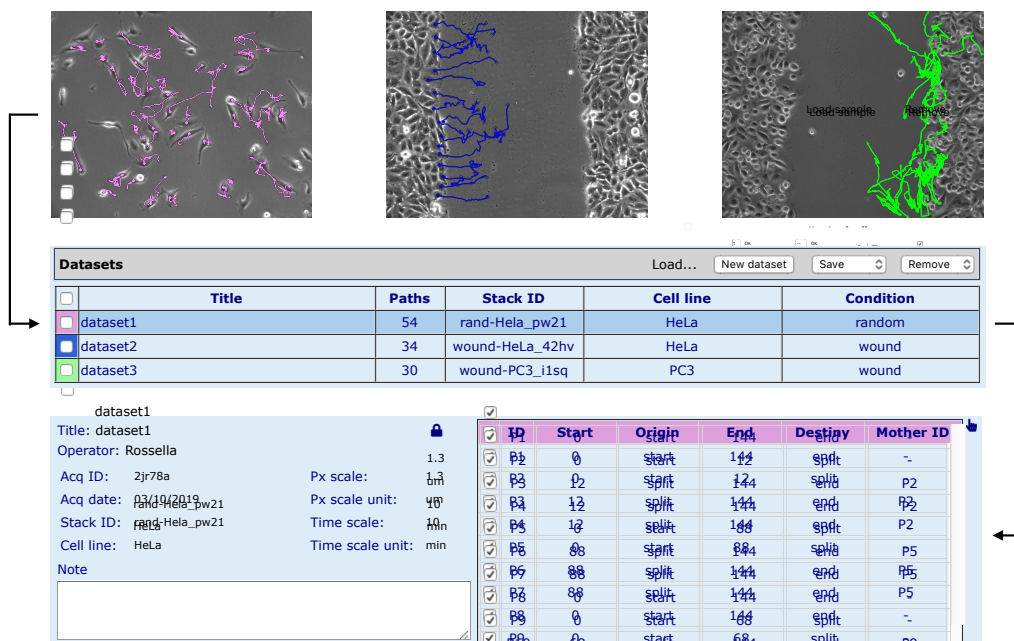


Figure 4.2.1 Multiple *movies* loaded within the application interface. The figure shows the two sections of the movie collection panel, the table section (middle) used to display the three loaded *movies* (top) and the *movie* detail section (bottom).

table includes the title and some essential features such as the number of tracked paths, the stack from which data derive, the cell line used and experimental conditions that indicate for example if an inhibitor has been used or a wound has been inflicted. At the top of this table have been included commands to load, remove, create and save datasets; to facilitate data feeding, the capability was added to upload a compressed zip file containing a number of coordinate files (*movies*). For each selected dataset, additional features are reported in the lower panel, for example acquisition ID and date, the pixel scale used and the time scale that indicates the frequency with which images were acquired, and also the name of the operator that performed the tracking procedure to build cell paths.

The collection of tracked cells has been organized into a table including, for each tracked cell, ID, origin, start and end time points, destiny and mother ID together with a link that generates the opening of a window showing the position and the shape assumed at each time point by the cell.

Movies and cell paths can be selected from the respective tables, by setting a checkbox which makes them available for further processing. In addition, cell paths can be automatically selected on the basis of their behaviour and features by using the selection system discussed in details under ‘4.3.3 Data selection and functional reorganization’.

4.3 Quantitative analysis of cell movement

4.3.1 A family of analyzers

The large number of analysis tools are available within the “analyze” panel, where they appear organized in six groups: ‘Culture’, ‘Cells’, ‘Time points’, ‘Model’, ‘Wound’ and ‘Stat test’ as shown in figure 4.3.1. The ‘Culture’ group includes analysis tools that extract descriptive parameters, such as average speed and direction of the cell population in exam. Under ‘Cells’, tools may be found that separately calculate movement parameters for each cell. The tools under ‘Time points’ estimate movement parameters in relation to time and allow virtual synchronisation of the observed cells. The ‘Stat test’ label groups inferential statistics tools that evaluate experimental data distributions and assess the goodness of fit. Models able to describe cell behaviour have been grouped under the ‘Model’ label and work by fitting mathematical models

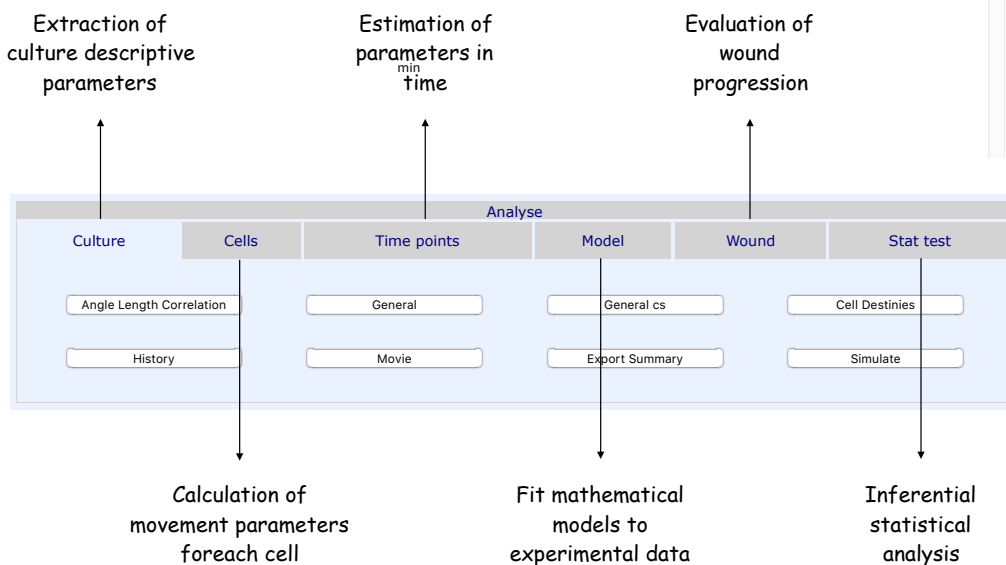


Figure 4.3.1 Panel of the analysis tools. This figure shows the panel through which the users can access to analysis tools, organised in six main groups selectable through the corresponding tabs: ‘Culture’, ‘Cells’, ‘Time points’, ‘Model’, ‘Wound’ and ‘Stat test’.

describing diffusive and persistent movement to squared displacements produced by cells from experimental cultures. The ‘Wound’ group includes analyses aimed to evaluate collective cell migration in wound healing experiments by two different approaches, the first starts from cell locations and evaluates the wound area as the fraction of smaller rectangular areas not occupied by cells, while the second works with the acquired images and is aimed to measure the wound area by differentiating cell covered pixels from

background pixels according to signal intensity. A description of the single analysis tools available in MotoCell is reported in table 4.3.1

Table 4.3.1 - The analysis tools.

Analysis tools	Description
Angle Length Correlation	Puts in relation step lengths and angles
General	Calculates population statistics for the whole recorded steps. Coherence bar plot for the whole recorded steps. Average step bar plot for the whole recorded steps.
General cs	Calculates population circular statistics for the whole recorded steps. Linear dispersion coefficient R bar plot for the whole recorded steps.
Cell Destinies	Shows origin and destiny for each recorded cell path. Origin and destiny for each cell are displayed in a line plot.
History	Displays cell status for each cell at each time point
Movie	Draws synthetic populations
Export Summary	Calculates the main descriptive parameters that allows to describe the mean behaviour of cell population
Simulate	Calculates the parameters necessary to simulate a synthetic cell population with the same features of the cell population in exam and interacts with the simulation tool
Path features	Calculates statistics for each recorded cell path. Direction and path length for each cell are displayed in a polar plot. Deviation/linearity scatter plot for each cell. Linearity/average step length scatter plot for each cell. Linearity scatter plot for each cell. Deviation scatter plot for each cell. Average step scatter plot for each cell.
Path steps	Displays step lengths for each cell and at each time point as well as average step for each cell and time point
Path angles	Calculates direction angle for each cell and at each time point as well as average angle for each cell and time point
Path cs	Calculates circular statistics parameters for each recorded cell path and plots linear dispersion coefficients (R) as a scatter plot
Volumetric Growth	Shows the volumetric growth of the cell population in exam
Step features	Calculates statistics by integrating all steps at each frame. Step length line plot in time
Step cs	Calculates circular statistics by integrating all steps at each frame
Rayleigh test	Executes Rayleigh test for linear dispersion coefficient R. Angular deviation and linear dispersion coefficient R in time are displayed in a linear plot
Proliferation	Calculates statistics and fit data using Weibull growth curves
Direction correlation	Evaluates the correlation between consecutive directions
Diffusion	Tests diffusive movement by calculating alpha and k coefficients from diffusion model for different time windows
Diff with bias	Tests biased random walk model for different time windows
Combined	Quantifies three movement features (random, persistence and bias) and their contribution to overall migration over time
Persistence	Tests persistent random walk model for different time windows
Levy walk	Performs a fit to Levy walk model. Normalized logarithmic bins of step lengths are represented together with the estimated Levy model in a scatter plot
Db manager	Builds a database of concentrations

Analysis tools	Description
Bioc Mod	Runs biochemical simulations
Evaluate trend	Evaluates data trend
Space fill	Calculates the wound area as the fraction of smaller rectangular areas not occupied by cells
Space fill 2	Calculates the wound area by image processing procedure, differentiating cell covered pixels from background pixels according to signal intensity
Cell segmentation	Calculates for each cell detected from fluorescence microscopy images the area, the perimeter, mean radius, minimum radius, maximum radius
Comparison parameters	Shows the more dependable than values
Normality test	Performs normality test for step length distribution. Step length histogram is represented together with the Normal and log-normal distributions.
Von Mises	Performs a fitting analysis between cell directions and Von Mises distribution. The directions are represented tighter with the Von Mises distribution function in a polar plot
Distribution fit	Performs a fit to six statistical distributions. The real and estimated distributions of step lengths are represented in a line plot

4.3.2 Data analysis in MotoCell

Figure 4.3.2.1 shows two examples of comparative analysis of 4 different cell lineages, HeLa, MDA, PC-3 and T24, stimulated by inflicting a wound in the

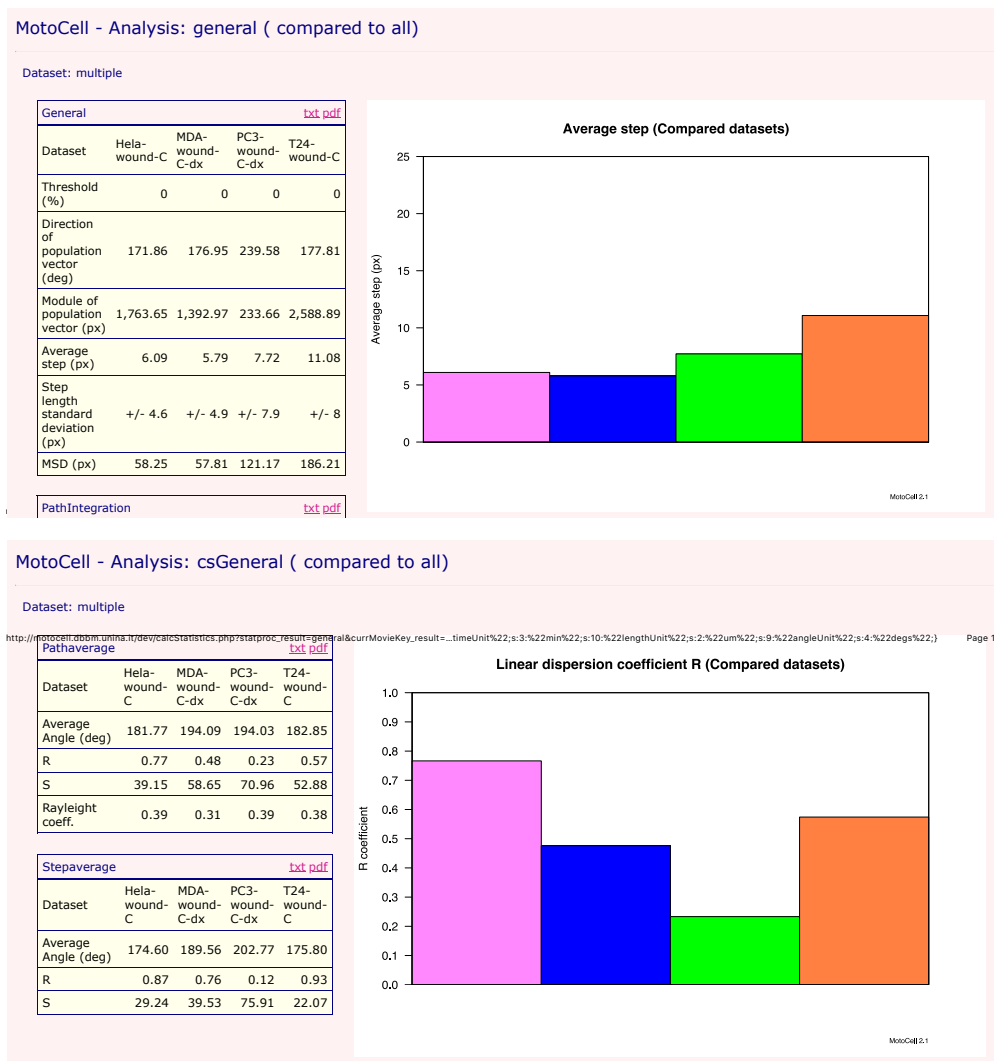


Figure 4.3.2.1 Estimation of descriptive parameters by MotoCell. This figure shows the output of two *analyzers* used to perform comparative analysis of HeLa, MDA, PC-3 and T24 cell cultures. The top panel is from the *General analyzer* and includes the comparison of basic motion parameters in table and graph form, while the bottom panel presents circular statistic parameters calculated by *General CS analyzer* also in table and graph form.

cell layer using the procedure described under ‘Materials and Methods’. For each cell line, general descriptive parameters in the top panel and circular statistics parameters R (linear dispersion coefficient) and S (angular dispersion coefficient) in the bottom one, are calculated and reported side by side in the tables. Average step length in top panel and linear dispersion coefficient R in the bottom one are also graphically plotted as a histogram. The results of the

analysis procedures, readily highlight the differences between the cell cultures, and show that HeLa cells (pink) move more slowly than T24 cells (orange), but with a stronger directional behaviour, demonstrated by the higher value of R coefficient and the lower angular dispersion coefficient S. PC3 cells (green) move faster than HeLa and MDA (blue) cells but their movement is less directional as shown by the much lower values observed for R coefficient. Figure 4.3.2.2 shows the results produced by two analysis procedures directed to investigate cell movement by evaluating step length (top) and path angle (bottom) distributions. In the top panel, step length distribution was evaluated

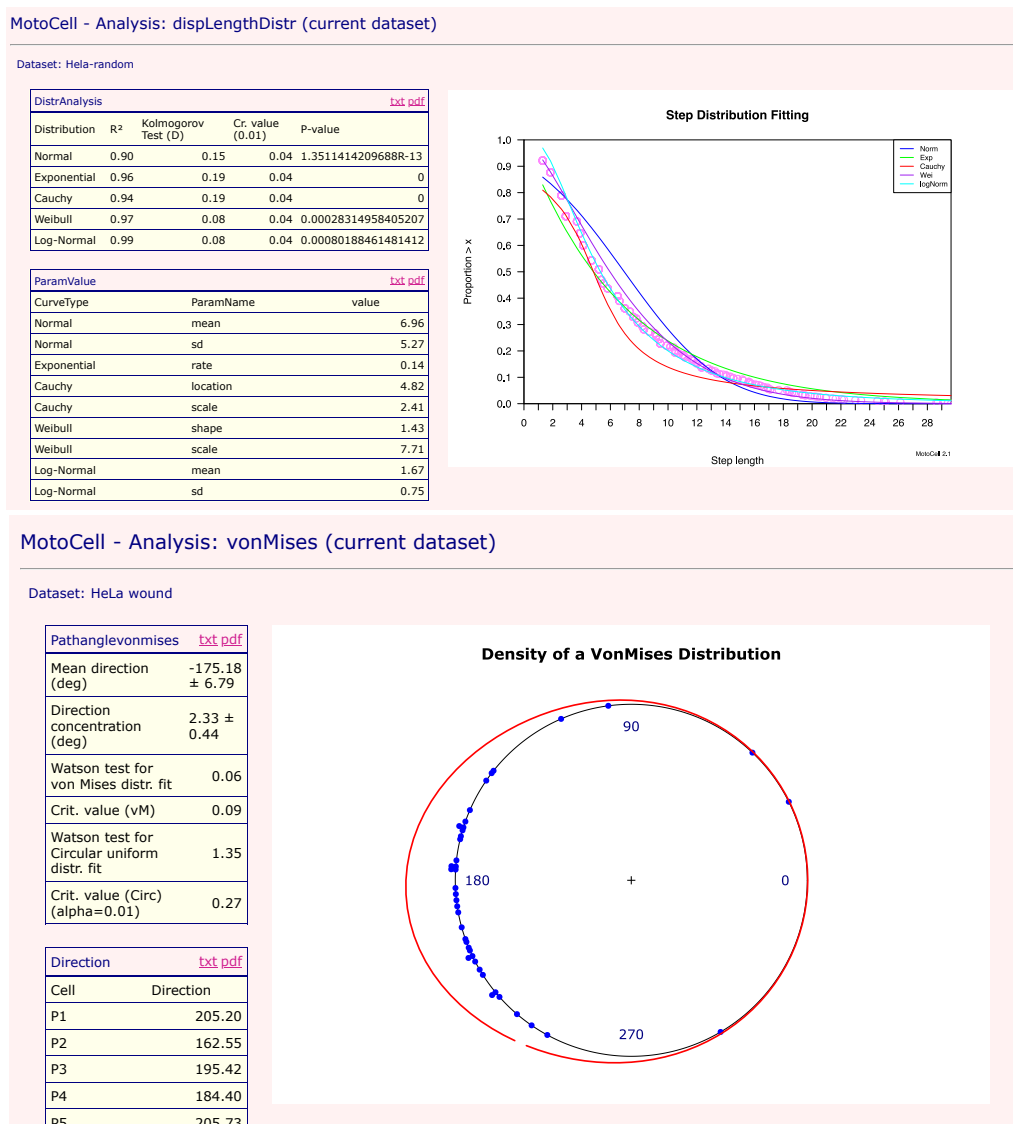


Figure 4.3.2.2 Analysis of cell movement by evaluating data distribution. Two examples of analysis procedures directed to investigate cell migration by evaluating length (top panel) and angle (bottom panel) distributions are reported. The top panel reports the results of fitting different distribution functions (Normal, Exponential, Cauchy, Weibull and Log-Normal) to step length distribution both in table and in graphic format. The bottom panel reports the result of fitting a Von Mises and a circular uniform distribution both in table and graphic format.

by fitting different distribution models (Normal, Exponential, Cauchy, Weibull, Log-Normal) to step length values obtained from a culture of HeLa cells moving “randomly” i.e. in absence of specific external stimuli. For each distribution model, the goodness of the fit is estimated by calculating R^2 determination coefficient and by applying the Kolmogorov-Smirnov test. In the reported experiment, the calculated R^2 determination coefficient indicates that a Log-Normal distribution, with mean equal to 1.67 and standard deviation 0.75, fits better than others with the length distribution of randomly moving HeLa cells. The analysis tool used in the bottom panel graphically displays path directions along a circle and helps investigate unidirectional movement by showing the results of fitting a Von Mises and a circular uniform distribution function to the observed cell directions. The von Mises distribution describes a unidirectional distribution of angles differently concentrated around a mean direction, while the circular uniform distribution describes homogeneously distributed angles. In the reported experiment in which HeLa cells have been stimulated by inflicting a wound in the confluent cell layer, the results indicate that cells move according to an unidirectional model, because the result of the Watson test is better (lower) than the corresponding critical value for the Von Mises distribution, and worse (higher) for the circular uniform distribution.

Figure 4.3.2.3 shows the results of a comparative analysis of normal NIH3T3 fibroblasts and transformed NIHRas, aimed to describe the two cell populations in terms of speed and directionality. The cells were followed after stimulation with a wound in the confluent monolayer, and according to distance from the wound edge, 3 groups of cells have been identified and separately analysed: ‘wound front’, ‘wound middle’ and ‘wound inner’. Cells grown without directional stimuli (random), but at low density, were used as a reference for the cell line. For each cell population, several (5 to 15) experiments were carried out and results are reported as a “box and whiskers” representation.

Speed of the population, expressed as the average step length walked by the cells at each time interval, shows that, for both NIH3T3 and NIHRas, the cells immediately close to the wound edge are faster than the middle and inner populations. The random populations are faster than the comparable inner populations, probably due to the combination of lower density in the plate and, for NIHRas, the effect of the oncogene constitutive activation.

The coherence of the populations and the linear dispersion coefficients (R) express the overall capability of cells to migrate in a coordinate way; “front” cells, faster, are also more sensitive to the wound stimulus and move with higher coherence and directionality than middle and inner cells. However, “middle” and “inner” populations, even if farther from the wound, are still sensitive to the stimulus with higher values of coherence and R than randomly moving cells.

The contribute of the “bias” component to total displacement is indicative of the capability of cells to respond to external stimuli, and, as expected, is very high for cells at the front, lower for middle cells and variably present in the inner populations. Cells moving randomly have a bias close to zero.

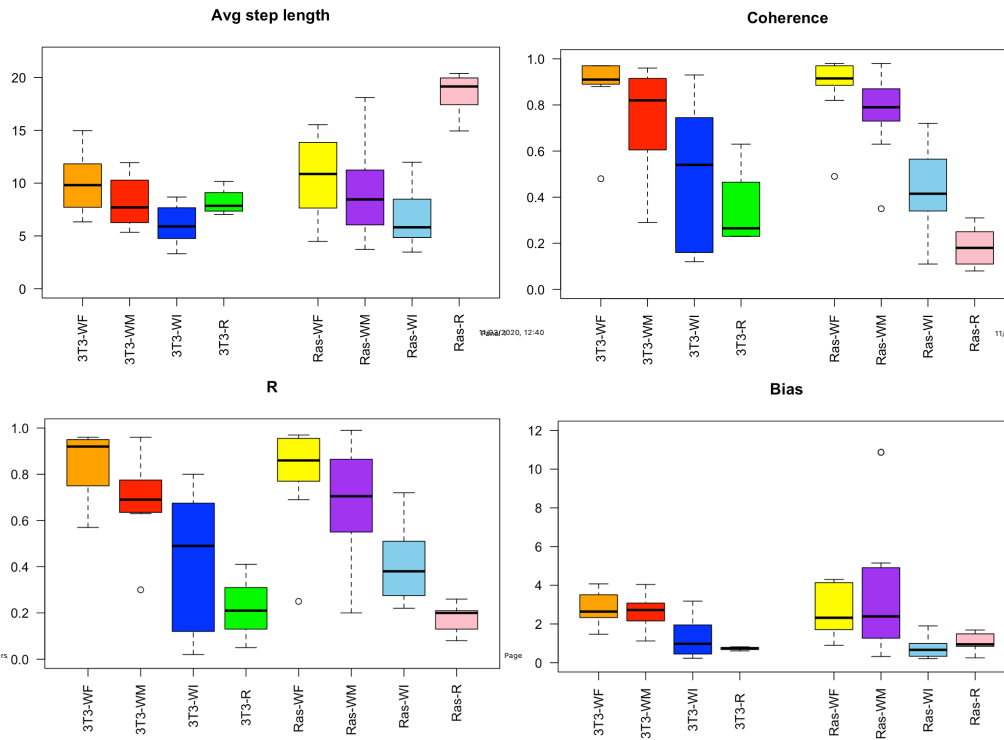


Figure 4.3.2.3. Comparative analysis of NIH3T3 and NIH3T3-Ras cells. Cell populations are stimulated by a wound and divided into 3 groups on the basis of their distance from the wound edge: ‘wound front’ (WF), ‘wound middle’ (WM) and ‘wound inner’ (WI); the reference population (R) was cultured at low density and without the wound. Top/left panel shows the distribution of average speed; coherence and linear dispersion coefficient (R) are in top/right and bottom/left panels respectively, while the contribute of the bias component to total displacement is in bottom/right panel.

4.3.3 Data selection and functional reorganization

Cell motility studies are typically performed on heterogeneous cell populations where individual cells show different features and behaviour, but sometimes homogenous subgroups of cells behave in a more consistent way. To separately investigate potentially homogenous cell subpopulations, a complex selection system has been designed and introduced in MotoCell (fig. 4.3.3.1). As a result, within the application, cell paths may be selected on the basis of a number of specific aspects of cell behaviour such as speed, location, movement direction, path length, life time as well as on the basis of their origin, i.e. cells present at the beginning of the observation (start) or appeared later in the observation field after a mitotic event (split) and/or of their destiny, i.e. cells

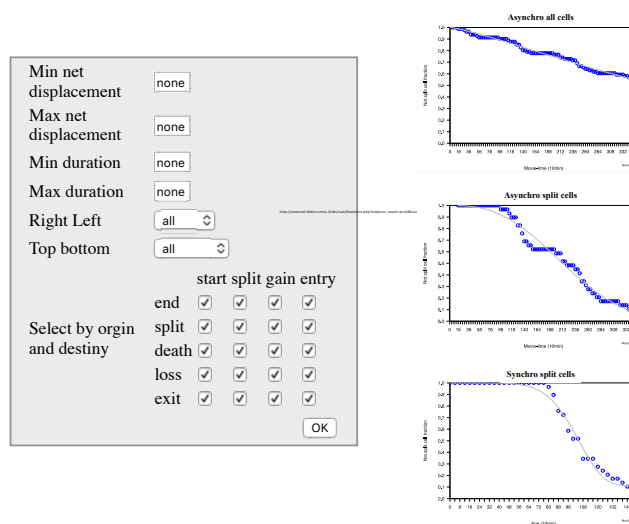


Figure 4.3.3.1 Data selection. This figure shows on the left the interface element that allows to select paths on the basis of the cell features and behaviour and on the right the growth curves obtained by analyzing different subset according to the acquisition time in the top and middle graphs and to cell age in the bottom one.

that undergo mitosis (split) or grow until the end of the observation. Cell path selection is carried out by using the selection system interface reported in the left panel of fig. 4.3.3.1. In the same figure (right) the results of calculating the fraction of unsplit cells, starting from all tracked cells (top panel) or from only the cells born during the observation time (middle panel), is plotted as a function of acquisition time. The bottom panel reports the same data as the middle one, but plotted as a function of cell age rather than acquisition time, thus resembling the growth curve of a synchronous population of the same type. The last plot may be used to estimate the probability, for each individual cell, of undergoing mitosis, and thus to calculate the “real” duplication rate of the population (see also ‘4.4 Evaluation of cell proliferation and its effects’). Analyses may be limited to shorter temporal ranges according to acquisition time, but also cell age, time that remains to live to the cells and percent of cell lifespan. These aspects can be chosen in the dialog box shown in fig. 4.3.3.2, in which analysis parameters are set and may be used to limit the requested analysis according to complex combinations of the above mentioned criteria. To implement this selection system, the *movie* object (see later under Architecture) has been extensively modified to support selective data retrieval. Next to the dialog box, fig. 4.3.3.2 shows examples of analysis performed by selecting according to different aspects. The dataset is limited to cells followed between two split events and average speed is evaluated in relation to acquisition time, age of cell and time remaining to live. The results show that after a split event (age panel) average speed is initially higher, but rapidly

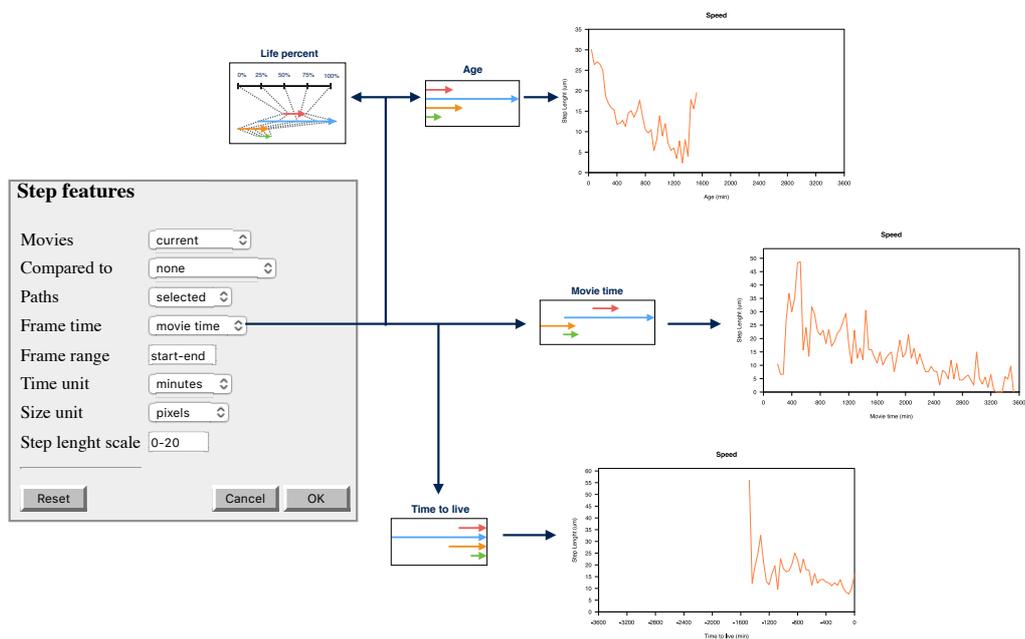


Figure 4.3.3.2 Data reorganization. This figure shows the dialog box by which analysis parameters are set. The user can choose to perform the analysis according to acquisition time, cell age, time that remains to live to the cells and percent of cell lifespan. On the right the average speed is evaluated as function of the cell age, acquisition time and time that remains to live.

decreases much faster than immediately before the next split (time to live panel), where the small speed decrease observed is comparable to that of the standard acquisition time based analysis (movie time panel). Comparative analysis are often performed by having one or more reference datasets compared to test experiments. To support this possibility all analysis tools can produce output results where control datasets are paired with test ones in different combinations: the current *movie* can be compared to all or selected *movies*, each *movie* in the selected collection can be compared to all or selected *movies*, all or selected *movies* can be compared with each other not giving particular emphasis to any specific *movie*.

4.3.4 Modelling tools describing cell movement

In MotoCell, tools have been added to study cell motion by fitting different movement models to experimental data describing speed and direction of all tested cells. The simplest test is based on a simple diffusive model (see Methods), by evaluating mean squared displacement (MSD) against time, as shown in fig. 4.3.4.1; in this model it is assumed that squared displacements

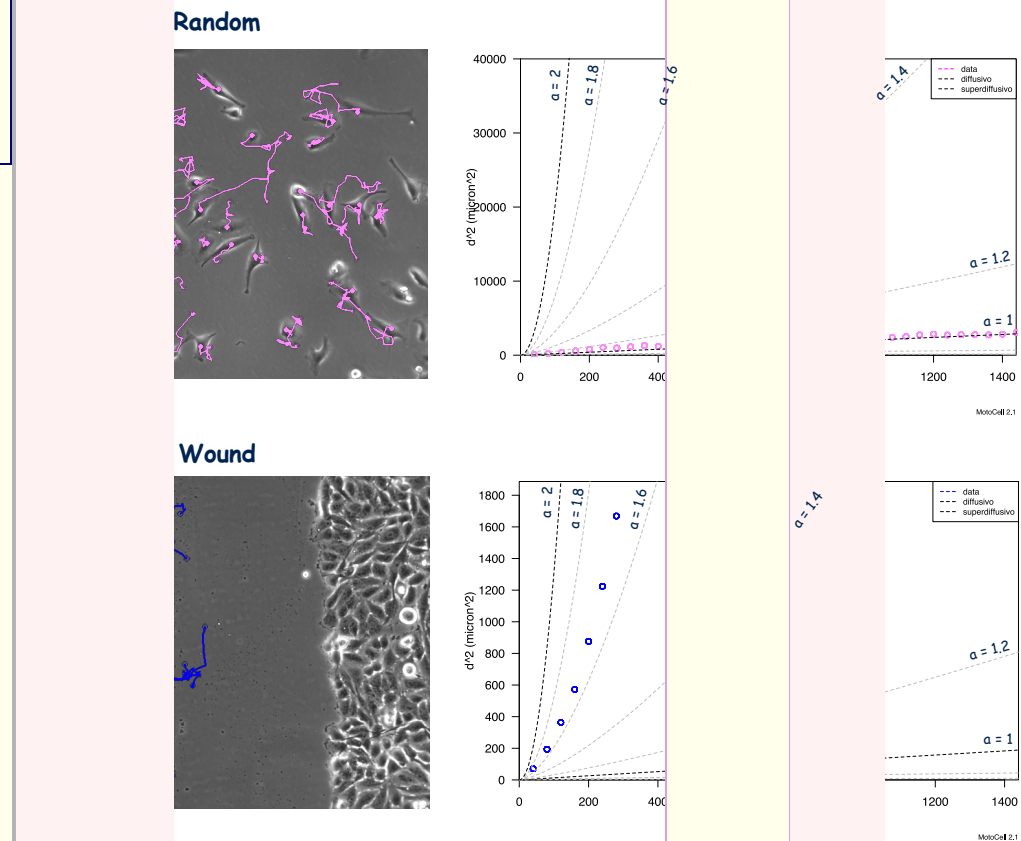


Figure 4.3.4.1 Evaluation of diffusive movement by curve fitting. The figure shows diffusion analysis performed on HeLa cells, maintained under standard conditions (top) and in presence of a directional stimulus (bottom). For both populations MSD is presented as a function of time in the graphs displayed on the right.

are proportional to time raised to a diffusion coefficient (α) ranging between 1 and 2, with 1 indicative of a perfectly diffusive behaviour, as those shown from randomly moving HeLa cells in the top graph, whereas higher values indicate a superdiffusive movement, as shown by HeLa cells observed following a wound stimulus in the bottom graph. Values higher than 2 are not frequently observed and would not be typical of continuous movement, as they imply some level of “jumping”, as for Lévy’s model.

Superdiffusive movement may be produced by different models, such as the persistent model, which relies on the concept that at any time interval, cells

move along a direction likely to be close to the previous one, unlike the purely diffusive model, which assumes that, at each time step, cells have equal probability to turn in all possible directions. In the persistent model, MSDs are related to the time by two parameters average speed S ($\mu\text{m}/\text{min}$) and persistence time P . Figure 4.3.4.2 shows the results of *persistence* analysis,

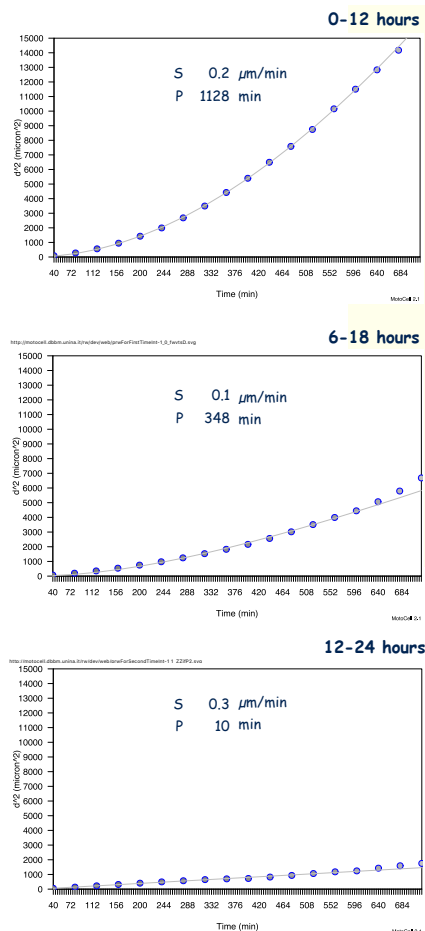


Figure 4.3.4.2 Study of persistent cell movement. The figure shows persistence analysis performed on HeLa cells stimulated by inflicting a wound in the cell layer. The three graphs report MSD vs time for three partially overlapping time windows as indicated at the top left corner for each graph.

performed on HeLa cells from a culture where directional migration is stimulated by inflicting a wound; persistence is higher for the first 12 hours as shown in the top graph and then it assumes lower values in two subsequent time windows reported in the central and bottom graph.

By using the above procedure, the right persistence value can be correctly obtained only for purely persistent movements, as for more complex movements this value could be easily overestimated by other components producing superdiffusive movement, such as a directional bias. To this aim an

analysis tool that models MSDs as the sum of three components (random, persistence and directional bias) was developed to separately estimate the contribution of each of the three components. Table 4.3.4.1 shows the results of using this model to evaluate movement of HeLa and NIH3T3 cells maintained

Table 4.3.4.1

	HeLa Random	HeLa Wound	NIH3T3 Random	NIH3T3 Wound
Random	6.09	6.05	9.41	7.61
Persistence	1.40	1.94	4.59	4.18
Bias	0.42	3.21	0.23	4.87
Mean step	6.13	7.30	10.51	10.31
Random contribution	5.8	4.87	8.38	4.59
Persistence contribution	0.20	0.81	1.68	2.51
Bias contribution	0	1.38	0.02	3.04

under standard conditions and under a directional stimulus (wound). For both cell lines, the wound results in a strongly increased bias, unlike persistence which is increased for Hela cells, but remains identical for NIH3T3 cells. Time based analysis, reported in figure 4.3.4.3, confirms this result, and allows to

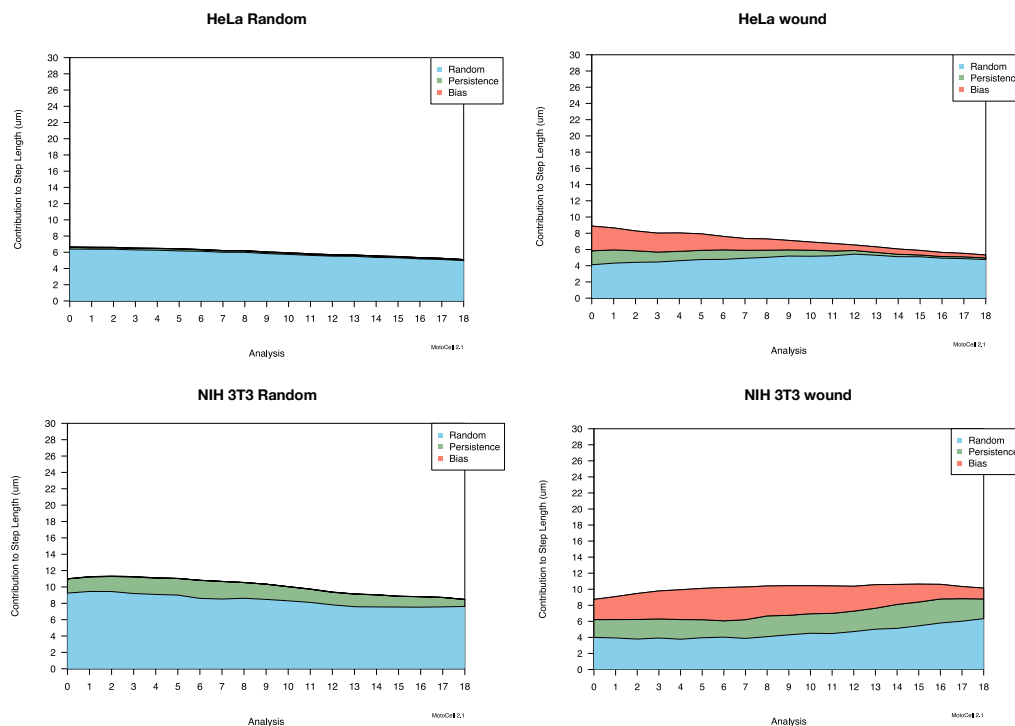


Figure 4.3.4.3 Study of cell movement by fitting a three component model In figure the contribute to average step length of each component (random, persistent, bias), calculated as described in ‘Methods’, is reported for HeLa and NIH3T3 cells maintained under standard conditions (left panels) and under a directional stimulus (right panels).

relate the superdiffusive component, given by the sum of the persistence (green) and bias (red) component, to the wound closure process. In the four panels reported in figure, at every timepoint, average cell displacement has been reported as sum of three component, respectively produced by random (blue), persistence (green) and bias (red). For HeLa cells maintained under standard conditions, the random component is predominant over the persistence one, which is very low, while bias, as expected, is absent. When a directional stimulus is introduced, persistence and bias components become considerably higher, but are progressively reduced as the wound is filled. The same analysis has been carried out on NIH 3T3 cells, which, unlike HeLa cells, move more as individually separated entities. In this case, cells show a higher persistence component clearly visible in both random and wound stimulated movement; as for HeLa cells, the bias component is strongly increased after a directional stimulus is introduced.

Figure 4.3.4.4 shows a comparative analysis directed to estimate the ability of NIH3T3 and NIH Ras cells to maintain the same direction in time which takes

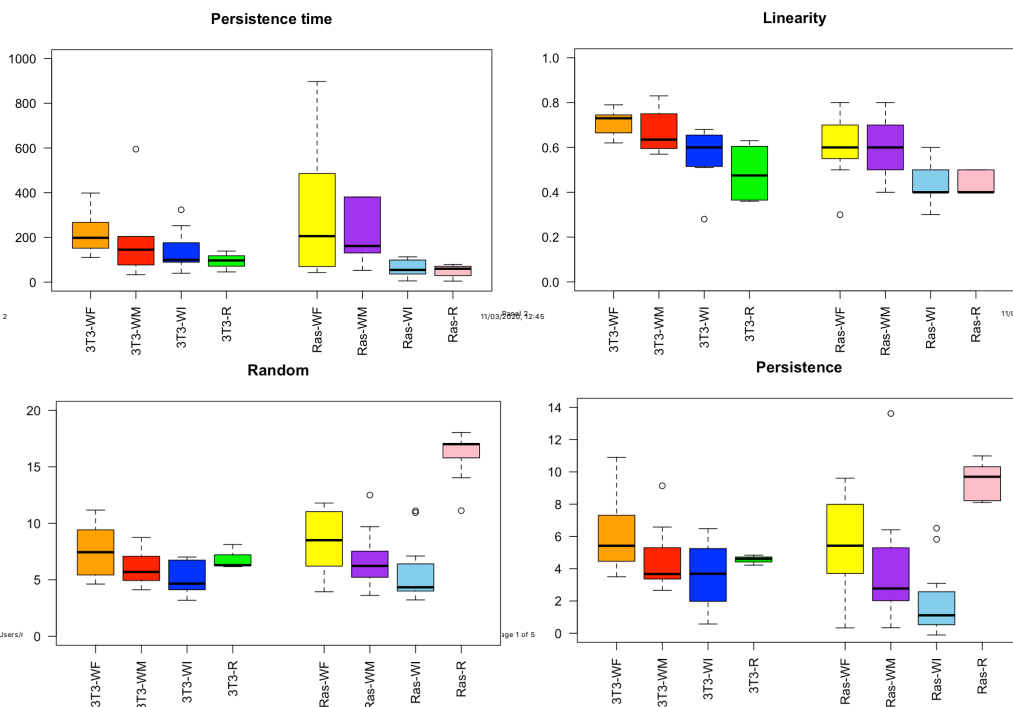


Figure 4.3.4.4. Comparative analysis of ability to maintain the direction. Top/left panel reports data about persistence time that is the time in which cell persists in the same direction; top/right panel reports data about linearity that express the winding of the cell paths; bottom/left and bottom/right graphs contains the distributions of random and persistence contribute to average step length.

advantage of different analyses. As already said for figure 4.3.2.3, for each cell population, several (5 to 15) experiments were carried out and results are

reported as a “box and whiskers” representation. Persistence time, evaluated as the time needed to lose the effect of the previous movement direction, progressively decreases from front to inner cells, although it should be considered that, as previously discussed, this measure also includes the effect of directional bias, which cannot be separated. The same is true for linearity, i.e. the ratio of net displacement to path length, which similarly is maximum in the cells located near the wound stimulus and progressively decreases in cells far away from the wound. Separate evaluation of random and persistence components contribute to average step length, calculated by the three component model described above under 4.3.4, shows more similar persistence components between the three cell layers, but highlights the different speed of the three populations. The same analysis gives evidence to the strong persistence of randomly moving Ras transformed cells, even in absence of any directional stimulus.

Figure 4.3.4.5 shows the same analyses carried out on NIH3T3 in wound healing assays, and highlights the effect of different signalling molecules on

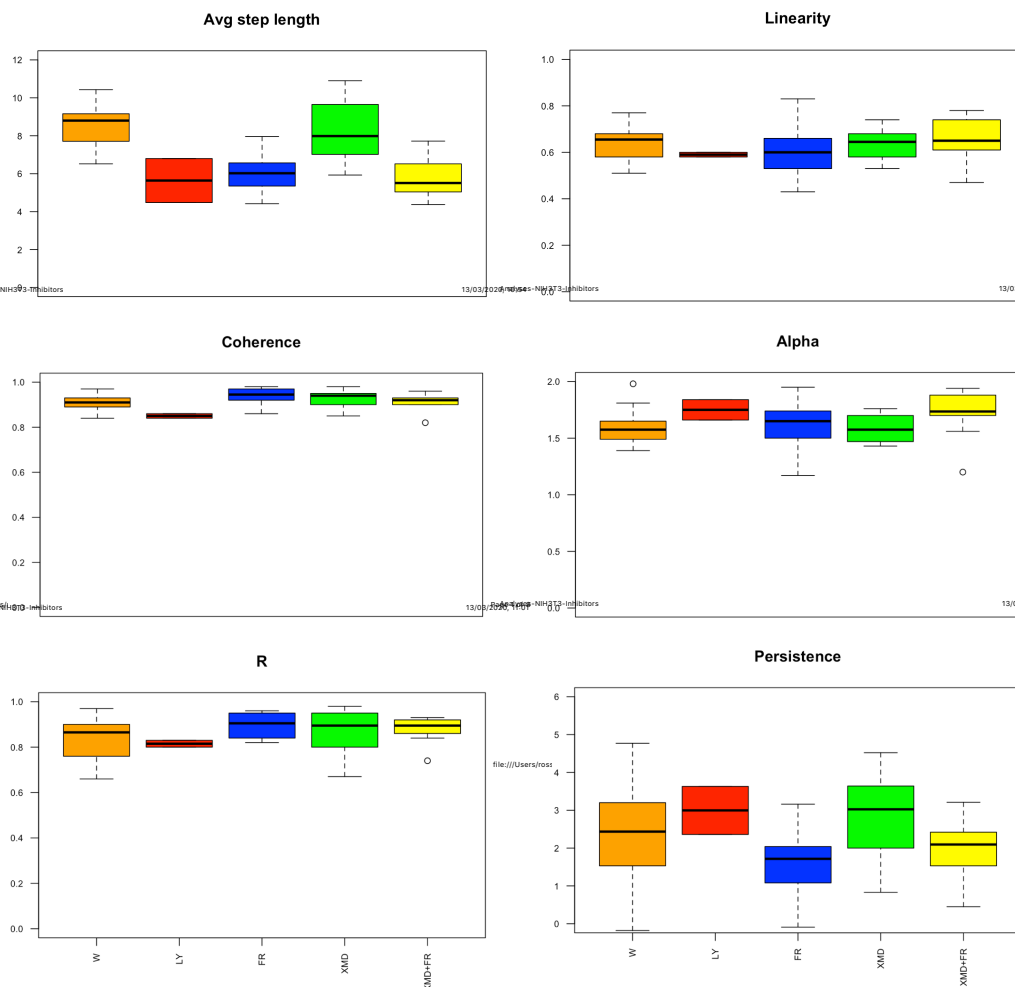


Figure 4.3.4.5. Role of signalling molecules on NIH3T3 movement features in wound healing assays. Wound stimulated cells were treated with LY, a PI-3 Kinase inhibitor, with FR180204 that blocks Erk1/2 kinase activity and with XMD-8-92, an Erk5 kinase inhibitor. Combination of the FR180204 and XMD-8-92 is also used.

specific movement features. Wound stimulated cells treated with LY, a PI-3 Kinase inhibitor, show a marked speed reduction, as seen in the “avg step length” panel, but no effect on directional parameters such as R, coherence and bias. Similarly, linearity and persistence are essentially unchanged. Blocking of Erk1/2 kinase activity by adding FR180204 appears to result in a specific loss of persistence, which is not shared by XMD-8-92, an Erk5 kinase inhibitor. No major effect is produced on coherence or R directionality indicators. Combination of the two inhibitors has the same effect of adding FR180204 alone, indicating that no interference exists between the two kinases. Finally, figure 4.3.4.6 shows a comparative analysis of a set of different cell lineages: NIH3T3 murine fibroblasts with normal phenotype, NIHRas murine

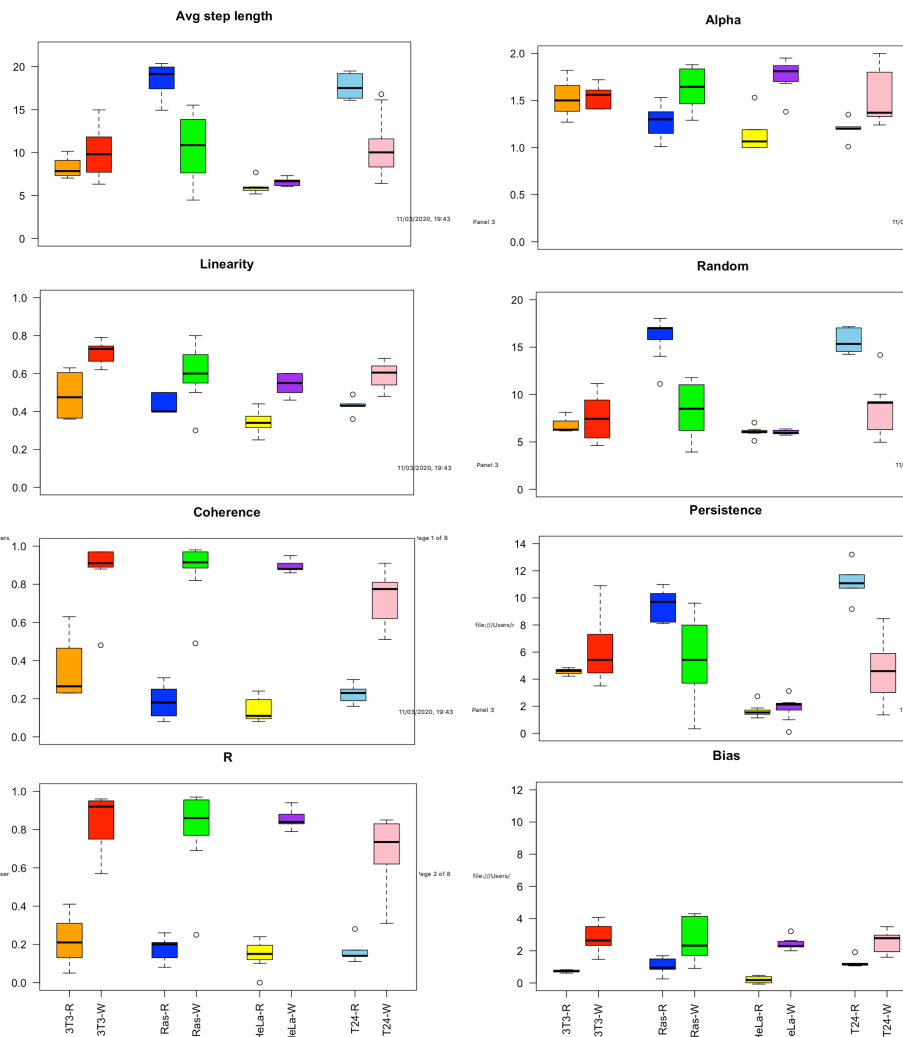


Figure 4.3.4.6 Comparative analysis of migration parameters of different cell lineages. NIH3T3 murine fibroblasts with normal phenotype, NIHRas murine fibroblast with transformed phenotype, HeLa from cervix carcinoma and T24 from bladder carcinoma, are compared under standard culture conditions and in presence of a directional stimulus (wound).

fibroblast with transformed phenotype, HeLa from cervix carcinoma, and T24 from bladder carcinoma, under standard conditions and directional stimulus (wound). All cell populations, when stimulated by a wound, show strong directional movement, indicated by higher values of coherence, R close to 1, high linearity, and evidence the contribute of directional bias to average step length. NIHRas and T24 cells, which both express constitutively activated Ras, show a characteristic, much higher, speed under standard conditions.

4.4 Evaluation of cell proliferation and its effects

When time-lapse experiments are followed for longer than a few hours, cells move but also tend to proliferate. In order to evaluate the contribution of proliferation in motility assay, an analysis tool has been developed in MotoCell, directed to quantify this aspect. The tool estimates replication rates of the culture by plotting the fraction of not split cells vs time and fitting a Weibull distribution (see in Methods) to these data (fig. 4.4.1). The Weibull distribution is used rather than a simple exponential one, as it can also fit to dataset whose growth curves show an initial lag.

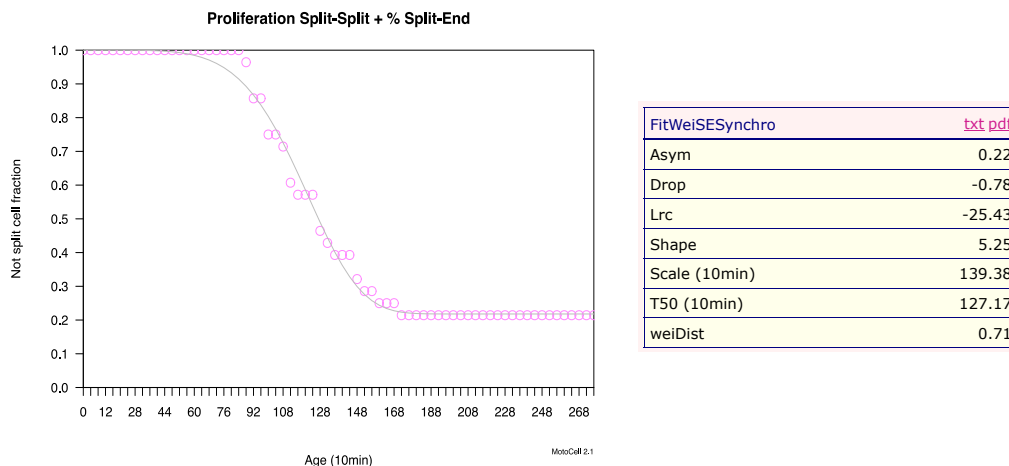


Figure 4.4.1 Quantitative evaluation of cell proliferation. In this figure an example of proliferation analysis is reported. On the left side the not split fraction of cells vs cell age is reported with the Weibull curve that better fit with data. The results of the curve fitting analysis are reported in the table on the right side.

The tool describes the proliferative behaviour of the population in terms of asym, the asymptote of the function that indicates the fraction of unsplit cells at the end of the observation, T50, the time at which 50% of cells are split, and shape, a parameter related to the shape of the decay curve (one for a purely exponential curve or larger for sigmoidal curves). In fig. 4.4.1 the same tool is used to determine the true T50 of a population, by limiting the analysis to cells born during the observation virtually synchronized at birth as described in 4.3.2. The parameters calculated by curve fitting are reported in the table; asym indicates that 27% of cells don't split at the end of the observation, T50, the time in which 50% of cells split, is about 19 hours.

4.5 Simulation of synthetic cell populations

MotoCell has been able to interact with a simulation system, developed in the hosting laboratory, to predict the behaviour of cultured cells in different experimental conditions observed in time-lapse experiments. The simulation

tool predicts the behaviour of single cells by using models able to describe the main cellular processes, such as movement, proliferation, growth and death. Populations ranging from tens to thousands of cells may easily be predicted within minutes or tens of minutes. Figure 4.5.1 shows the interaction of

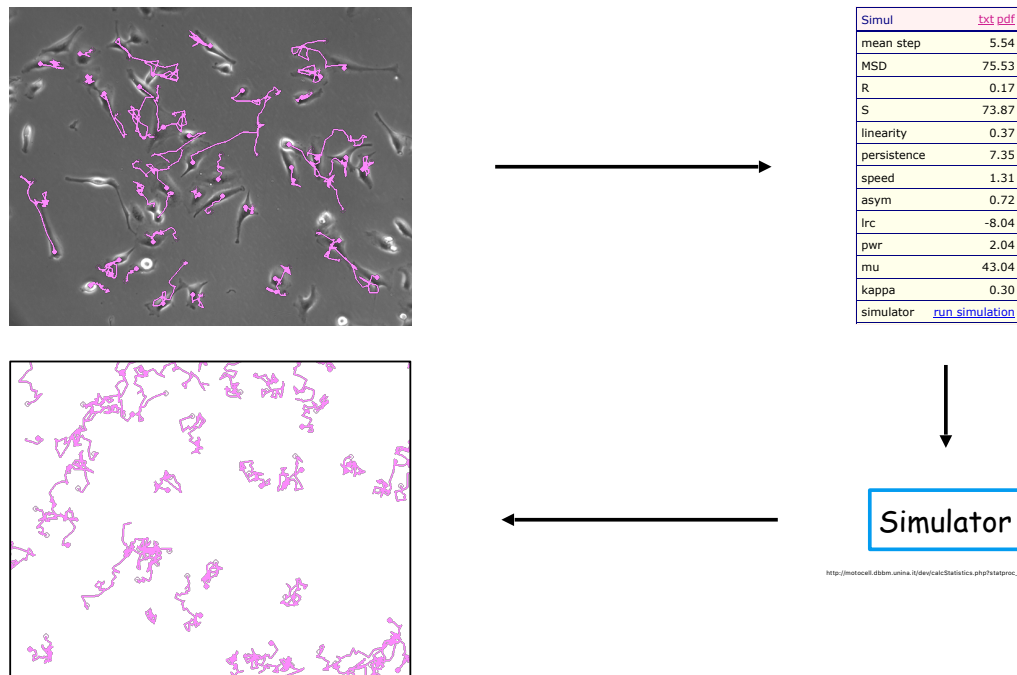


Figure 4.5.1 Interfacing the simulation tool with MotoCell. This figure shows a schema which describes the flow according to which MotoCell and the simulation system interact. The movement and proliferation parameters calculated from a coordinate file derived from an experimentally observed cell population are passed to the simulation tool that in turn generates one or more synthetic cell populations sharing the same features of the starting population.

MotoCell with the simulation system: typically, a coordinate file derived from an experimentally observed cell population is analyzed and the parameters calculated are ‘passed’ to the simulation system that in turn generates one or more synthetic populations sharing the same features of the starting cell population. Before executing the simulation one or more parameters may be changed, trying to predict the behaviour of the same cell population in response to changed conditions, such as after a mechanical and/or biochemical stimulus. The results of a simulation is a dataset contained in a *movie* file that is loaded in MotoCell to be analyzed, for example, compared to the experimental dataset. As shown in figure 4.5.2, feeding the data derived from MotoCell *analyzers* to the simulation system, different movement patterns are generated (middle row), which closely resemble those observed for the experimental cell populations from where the parameters were obtained. The results are

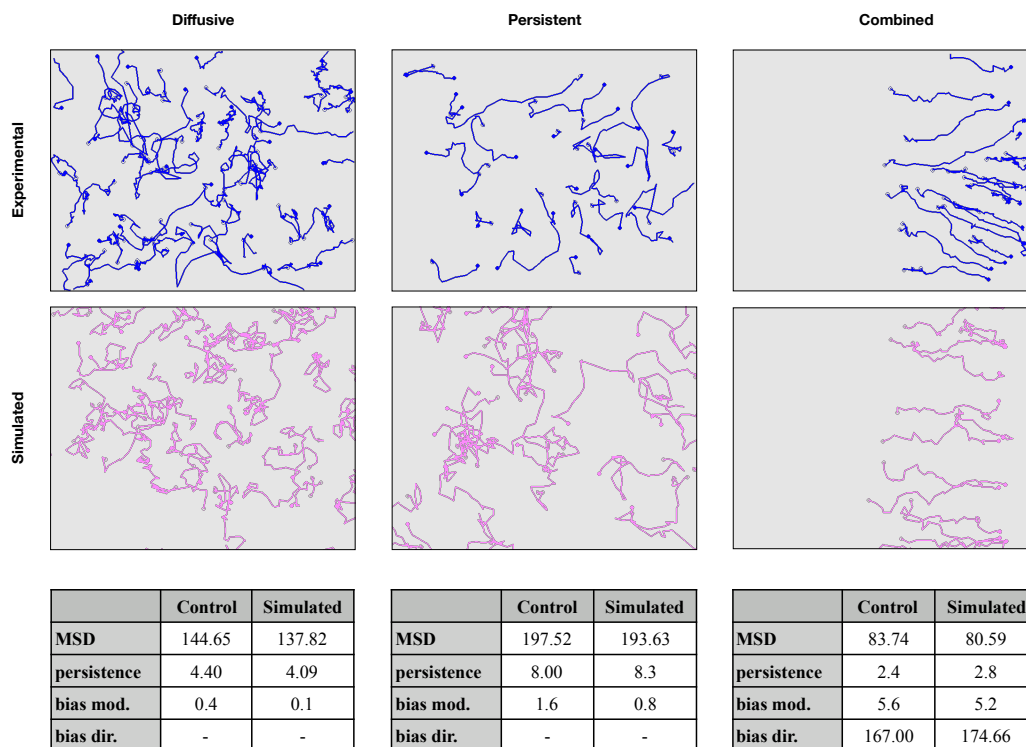


Figure 4.5.2 *In silico* experiments. The figure reports the paths calculated for three synthetic cell populations characterised by diffusive (left), persistent (middle) and combined (right) movement, built by using the parameters calculated for three experimental cell populations. The top and middle rows respectively display the paths observed with the experimental populations and calculated for the synthetic populations. The bottom row shows numerical parameters calculated from both experimental and synthetic populations.

confirmed (bottom row) by noting that mean squared displacement, persistence and bias module/direction calculated for each dataset closely resemble those produced by evaluating the same parameter for the corresponding original populations.

In addition procedures to model cell profile while cells adhere and move and to visualize simulated datasets have been added. All cells after the seeding are detached and considered like spheres that fluctuate in the medium, then when cells anchor the substratum are still spheres but stop to move. Once that cells adhered, after about an hour, they start to spread and to assume a more irregular profile reproducing membrane ruffles and to increase their size. In this phase mean cell radius is calculated by multiplying the radius of a sphere with the same volume of the cell by square root of a spreading factor. Once that spreading factor reach its maximum value the cell is completely spread and assumes the typical shape of its cell type. When cell starts to move its profiles is evolved according to the movement by adding protrusions that justify the movement and removing the others that are not compatible.

Within this work, keeping the architecture in tune with the original project principles, many objects were modified and others added to make MotoCell an effective tool to quantitatively study in parallel cell movement in many time-lapse experiments by integrating the calculation of movement and proliferation descriptive parameters, the fit of movement models to experimental data, the execution of *in silico* experiments and the visualization of many image stacks with the cell paths.

4.6 Motocell architecture

MotoCell is a web application written in PHP, and uses two main html pages: the main one (index.php), to display and edit images and paths, and to request all analysis procedures, and a second page (calcStatistics.php), used to generate all analysis results. Additional web pages are used to display dialogs, used to acquire optional parameters necessary for the execution of most analyses, and to recover data stored on Server, such as images or movies. Storage space is used to keep temporary copies of images and datasets, to store the current application status, to keep track of used ids, to store images and graphic plots waiting to be downloaded by the clients.

4.6.1 Objects hierarchy

Most code is contained in a number of objects, developed to support specific functions and reported, as an inheritance hierarchy, in figure 4.6.1 The main

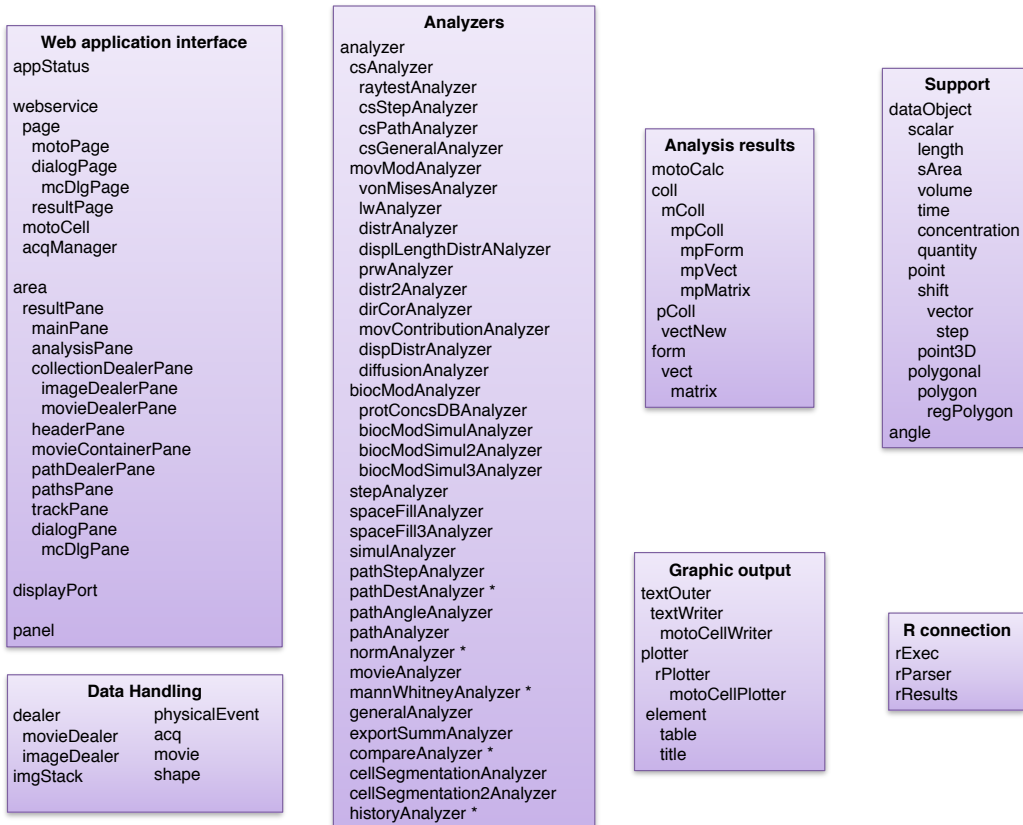


Figure 4.6.1 Objects hierarchy. The figure shows the objects used by MotoCell, grouped in 7 main hierarchies: ‘Web application interface’, ‘Data handling’, ‘Analyzers’, ‘Analysis results’, ‘Graphic output’, ‘Support’, ‘R connection’.

object subfamilies include those for building the web interface, including several “page” and “pane” objects, a family of data handling objects, used to deal with image stacks and movies, a large family of analyzers, responsible for most analysis procedures, a set of objects for generating variously formatted text and plots to be used for graphic output. Additional sets of objects include data objects used as containers for analysis results, and a family of data objects used as support for representing physical entities involved in cell movement. Interfacing with R is provided by a small set of objects that execute R scripts and convert input and output data.

MotoCell interface was organized using 5 panes, described in 4.2.1: for each pane, the html code is generated by a specific object that extends a parent *area* object, that handles also the store of variables related to its own status. The

panes that collect image stacks and coordinate files are used by two objects that handle data collections, respectively the *imageDealer* and *movieDealer* objects. *imageDealer* collects and manages image stacks as *imgStacks* objects, while *movieDealer* stores and handles cell tracking data as *movies* objects. Image dealer pane and movie dealer pane communicate with the panel that manages editing, display and cell tracking by tools presented in dropdown menus, to determine data on which operate. Access to the analysis system is through the “analysis pane” acting as the access point and through which data, selections and application status are passed to *analyzers*, to enable them to carry out the respective analyses. An intermediate dialog page allows to customise the behaviour of most *analyzers* by setting specific optional parameters. The ‘graphic output’ objects are used to assemble the final web page with tables and plots.

4.6.2 Data objects

Movement parameters expressed in standard units of measurement are essential to compare different experiments, considering that the dimension of the pixel can change between an experiment and another and consequently using measurements expressed in pixels would make the results not comparable: image stacks from which cell paths are obtained can in fact have different pixel scales and positions tracked for each cell, are stored in pixels in the application and coordinate files. To help solving this as well as other problems in handling physical entities such as locations and displacement vectors, a set of *dataObject* objects were developed to manage the entities involved in analysing cell morphology and migration patterns, such as position, shape, time. These objects manage the mathematical operation between physical quantities expressed in the same or different units and allow the retrieval of data in the required unit of measurement by taking care of the conversion between arbitrary values, expressed in arbitrary units, and physical objects characterised by a specific unit of measurement.

4.6.3 Interfacing with R

R (website: [R](http://www.r-project.org/)) is a data analysis environment originally designed to support statistical analyses, but later extended to support applications in wider contexts, including physics, mathematics, image analysis, bioinformatics among others, by providing data analysis tools and graphic routines. In order to take advantages of its functionalities, for example for estimating curve fitting parameters or to use statistical tests, an interface was built which could transparently pass data and recover the results after executing R routines and functions. The interface, based on the *rExec* and *rResult* objects, was developed to facilitate the execution of R scripts in MotoCell by indifferently using a local R instance installed on the web server or a remote one, accessed

via Rserve (Urbanek, 2003). The analysis performed in MotoCell has no need to change script or input data according to the execution mode, as *rExec* builds the final script to be executed in R by adding up input data, script content and variables to be sent in return before running the script. As a result, R scripts receive input data and return the results in variables thanks to functions added to the main analyser object and readily available to all analysers modules that manage the analysis procedures (see below).

4.7 The analyser objects: MotoCell as a development environment

The large number of analysis tools available in MotoCell was implemented by using a modular structure, where each set of related analysis tools is included in an object that acts as a plugin module containing all the information and the behaviour necessary to add the tools to MotoCell.

4.7.1 The analyzer objects

Figure 4.7.1 shows how *analyzer* objects have been organized. A parent *analyzer* object with no interface, i.e. not appearing in the *analyzers* panel, contains the basic functions and all *analyzer* objects acquire these functionalities by extending it.

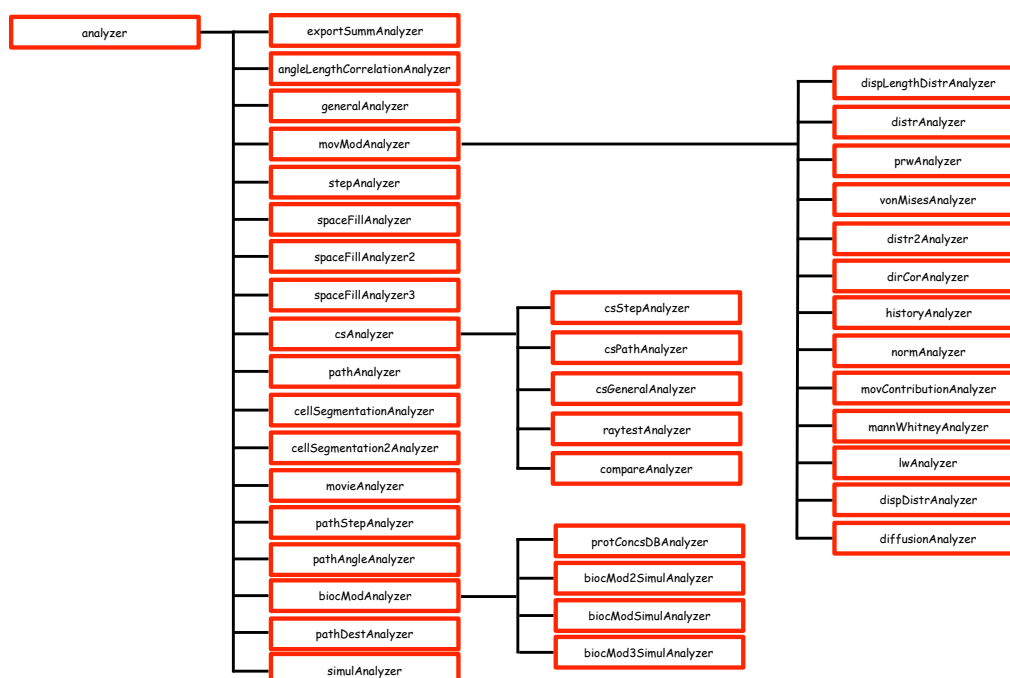


Figure 4.7.1 Hierarchy of analyzers. The image shows the hierarchy of *analyzers* objects currently available in the application. A parent object *analyzer*, contains all the basic functions that are acquired by all *analyzers* objects that extend it. Some of them are parent objects of other *analyzers* such as *movModAnalyzer*, *csAnalyzer* and *biocModAnalyzer* that respectively contain the functions to extract mean squared displacements (MSD) for the routines that test mathematical models, to calculate circular statistics parameters and to support biochemical pathway simulations.

Current *analyzers* either directly extend the base *analyzer* object, or another *analyzer* (with or without interface) which includes common routines. To this aim a parent object *movModAnalyzer* was built to extract and/or calculate value sets such as mean squared displacements (MSDs) vs time, that are then used as input data by other *analyzers* such as *diffusionAnalyzer* and *prwAnalyzer*;

respectively testing the diffusive and persistent random walk movement model by fitting the relative models to MSDs. Similarly, *csAnalyzer* is the parent object developed to calculate circular statistics parameters such as linear dispersion coefficient (R) and angular dispersion coefficient (S); these routines are used by other *analyzers* extending it, such as *csGeneralAnalyzer*, *csPathAnalyzer* and *csStepAnalyzer* to calculate R and S respectively for the population, for each path and for each time point. In addition, in an initial effort to introduce simulation of biochemical pathways, another parent object *biocModAnalyzer* has been built to estimate and retrieve concentrations of molecules involved in a specific biochemical pathway on the basis of the cell line. These data are used for example by analyzers as *biocModSimulAnalyzer* to carry out specific simulations.

4.7.2 Services and functionalities available to analyser objects

As shown in figure 4.7.2.1, the basic functions available to all analyzers allow to determine how it is presented in the analyses pane, how to organize the

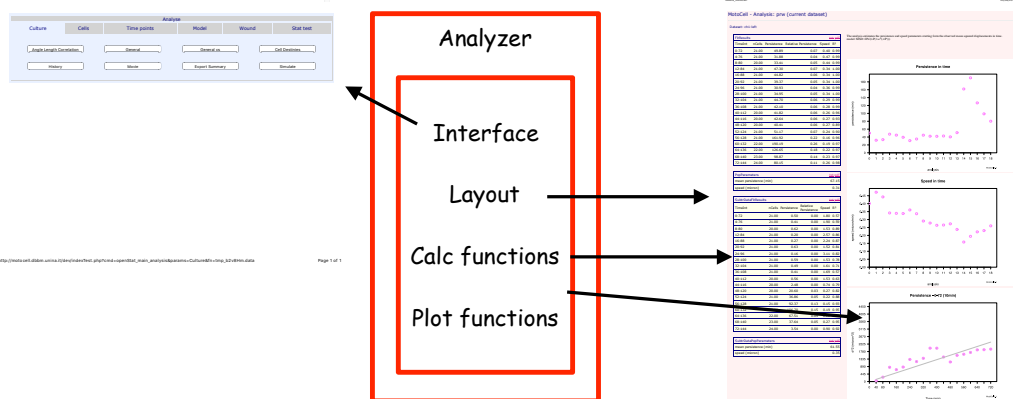


Figure 4.7.2.1 Analyzer functionalities. An *analyzer* object always contains functions to determine its interface in the analysis pane, to organise the results in the final page, to calculate and to plot data, in addition to functions deriving from the specific nature of the performed analyses.

layout in the result page, basic calculations to calculate movement and proliferation parameters and to plot data.

Each analyzer object provides routines for data processing and for generating output elements, such as tables and plots. The analyzer system provides means of caching intermediate results: in this way results calculated for a given output may be reused for different outputs or for other calculations, reducing the execution time of analysis tools, a feature which is particularly effective when many large datasets are analyzed in parallel.

By using the *rExec* method, analyzers have access to the whole R environment

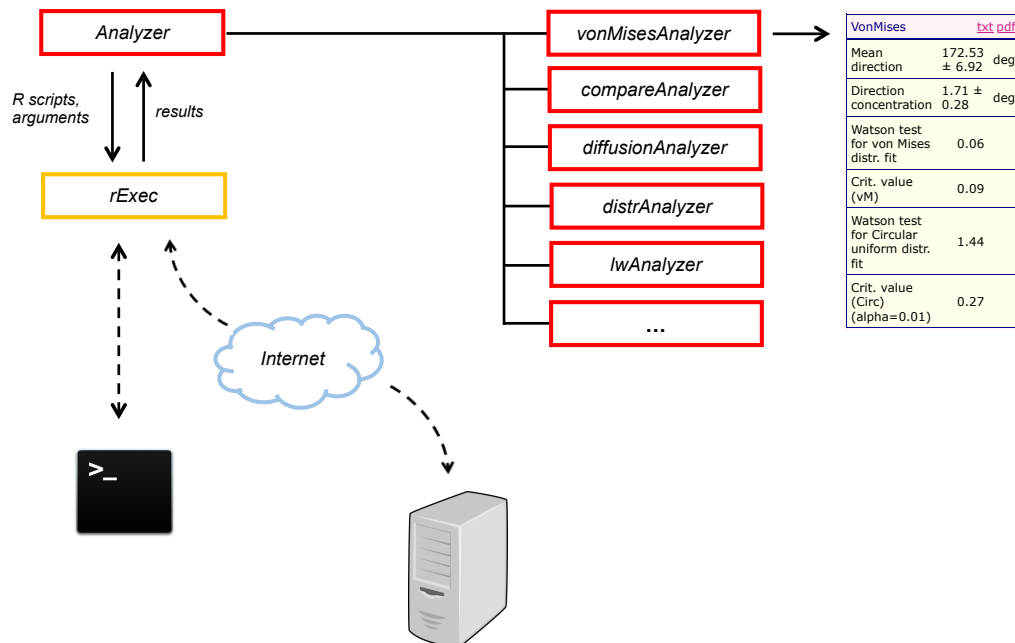


Figure 4.7.2.2 Interfacing with R. The figure shows the interaction between *analyzer* object and *rExec*. An *analyzer* sends to *rExec* the R script to execute, the necessary input data to run it and the list of the variable to retrieve, the *rExec* runs the code by using an R instance locally installed on the web server or one installed on a remote server accessed via network and returns the results that are to be used by the *analyzer* for further processing or display in the output tables.

to execute scripts, with the analyser system taking care of passing arguments and retrieving results.

rPlotter, a new object developed to deal with graphic data representation, also uses R functionalities, to produce a relatively large set of graphs able to highlight trends, changes and relationships. Results calculated by *analyzers* can now be plotted with the support of *rPlotter* that, after receiving by an *analyzer* input data to plot and all the features necessary to build the plot such as the plot type (line, bar, polar), the main title, X and Y axis titles, the colors to represent datasets, builds the script to pass to *rExec* to generate the graph, as shown in Figure 4.7.2.3.

The introduction of a get-image web service has added the possibility of directly processing acquisition images within the analyser system, rather than operating on numeric data contained in *movie* files. Scripts executing in R can use R image analysis functions in R scripts via a strategy devised in MotoCell, to “pass” images through *getImage*, a web service that returns an image defined by a stack ID and a frame. Figure 4.7.2.4 shows how the modules interact in the case of an analysis that requires image analysis functions: a list

of URLs that point to the *getImage webservice* is passed as input data to *rExec* and R subsequently uses the URLs as file identifiers to pass to image analysis functions.

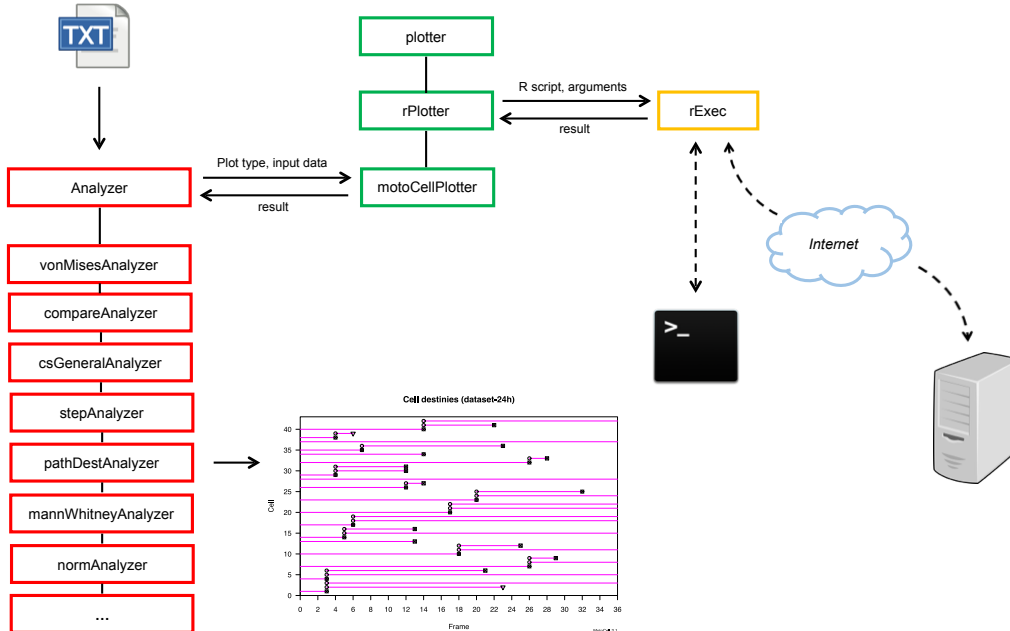


Figure 4.7.2.3 Using R for graphic representation of data in MotoCell. The image shows the flow to generate graphs with the support of R functionalities.

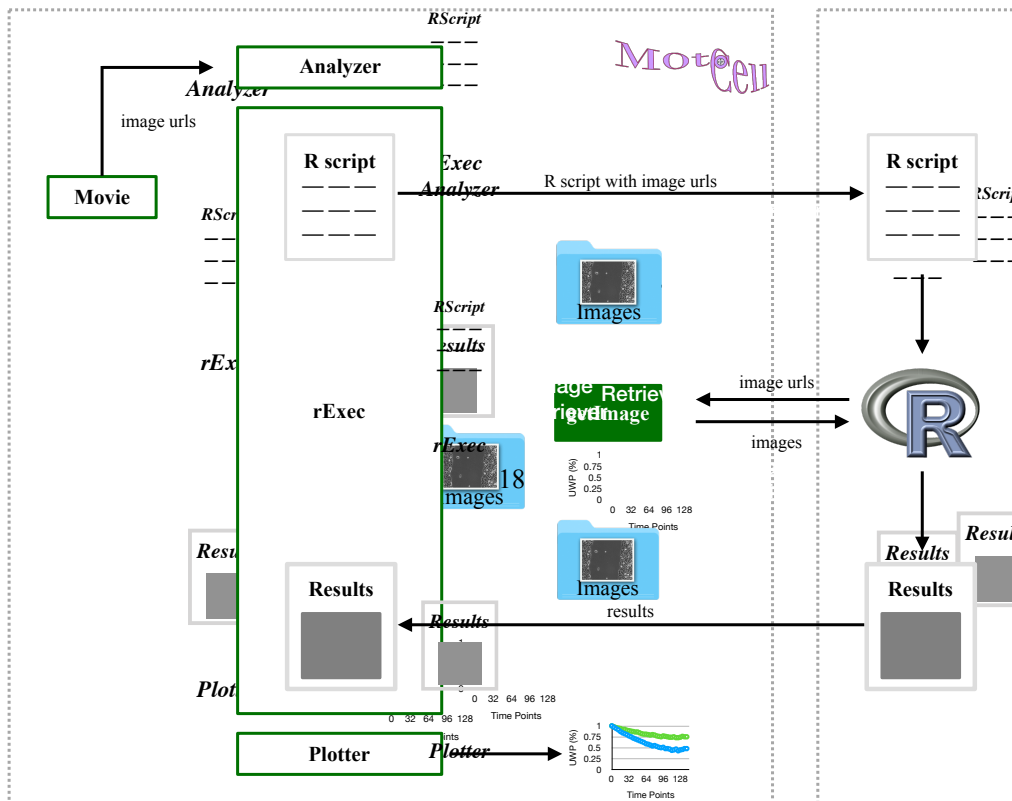


Figure 4.7.2.4 Image analysis with R in MotoCell. The figure shows a schema depicting how the modules interact when an *analyzer* carries out functions to analyze images by using R functions.

The recent development of this model, combined with the modifications introduced in the *analyzers* to analyze cell tracking data and images, the possibility to easily and transparently access R functionalities, the ability to produce output tables and graphs are turning it into a development environment in which new analysis procedures may be easily created and tested, taking advantage of the many services provided by the package, also by people who are not part of the development team.

5. CONCLUSIONS

An integrated environment was developed to study cell migration by combining time-lapse experiments and computational analysis. The environment is composed of different modules and is based on MotoCell, a web application that can manage images contained within acquisition files, produce, display and edit text files containing the paths followed by individual cells and analyze the data by a number of different statistical analyses.

Within MotoCell, different time-lapse experiments can be simultaneously managed and comparatively analyzed to highlight similarities and changes among different experiments. Analysis may be restricted to specific sub-population thanks to an intelligent selection system which allows to select cells on the basis of their behaviour and features such as path length and direction, life time, origin and destiny. In addition, the behaviour of cells may be investigated as a function of acquisition time, their age, time that remains to live and percent of lifespan and by limiting the temporal ranges.

The possibility to acquire from time-lapse microscopy image stacks information about each single cell by tracking procedures combined with the capability to select cells on the basis of their features, allows to investigate the movement of specific subgroups in order to characterize homogeneous cell populations and to investigate similarities and differences among different groups. Cells that belong to different groups can respond differently to drugs, so, knowing the heterogeneity in a cell population, it is possible to test and hopefully set up more efficient therapeutical strategies.

Mathematical models describing various types of movement may be tested by performing curve fitting analysis to test different movement and proliferation models. Curve fitting parameters may be used to simulate specific cell cultures able to reproduce the behaviour of cultured cells observed during time-lapse experiments and to predict their behaviour in response to mechanical or biochemical stimuli. Within MotoCell, mitosis events may be recorded, stored and analyzed in order to estimate the contribute of cell proliferation to motility assays.

The environment has been developed to enable comparative analysis of multiple experiments simultaneously. Overall, these capabilities may be used to highlight similarities and differences among different experiments and to compare and evaluate the effects of drugs, to investigate biochemical pathways involved in cell movement, to characterise the effects of mutations in molecules that affect cell movement and morphology, to highlight similarities and differences among cell lines that originate from the same or different tissues.

In its present form, thanks to its object oriented structure and to the modular organisation of *analyzer* objects, the system also acts as a development

environment, in which routines such as those able to extract, reformat and select data, access the R environment, output result sets in tables and graphics, are easily available and provide support for the generation of custom designed *analyzer* objects.

6. ACKNOWLEDGEMENTS

I would like to express my sincere gratitude to my tutor, Professor Giovanni Paolella, for supporting me during the entire PhD period, for his patience, motivation, and immense knowledge. I could not have imagined having a better advisor and mentor for my PhD study.

I would like to thank Leandra Sepe for her suggestions, comments and valuable advice, which helped me to widen my research from various perspectives.

I also would like to thank Angelo Boccia that has helped me in the early stage of this project and has continued to be a 'point of reference' for me.

I would like to thank Elvira Toscano who has on several occasions helped the development of the project with enthusiasm and dedication.

I wish to extend my special thanks to Rocco Caggiano and Elena Cimmino for the stimulating discussions, their sincere friendship and their constant support.

I would like to express my deepest gratitude to my family that has always supported me unconditionally, with patience and love.

7. REFERENCES

Al-toub M, Vishnubalaji R, Hamam R, Kassem M, Aldahmash A, Alajezi NM. CDH1 and IL1-beta expression dictates FAK and MAPKK-dependent cross-talk between cancer cells and human mesenchymal stem cells. *Stem Cell Research & Therapy*. 2015;6:135

Ananthakrishnan R, Ehrlicher A. The forces behind cell movement. *Int J Biol Sci*. 2007 Jun 1;3(5):303-17. doi: 10.7150/ijbs.3.303. PMID: 17589565; PMCID: PMC1893118

Anderson, A.R.A. and Quaranta, V. (2008) Integrative mathematical oncology. *Nat. Rev. Cancer* 8, 227–234

Arocena M, Zhao M, Collinson JM, Song B. A time-lapse and quantitative modelling analysis of neural stem cell motion in the absence of directional cues and in electric fields. *Journal of Neuroscience Research*. 2010;88(15): 3267-3274 *Time-Lapse Microscopy* 53 <http://dx.doi.org/10.5772/intechopen.81199>

Bago JR, Alfonso-Pecchio A, Okolie O, Dumitru R, Rinkenbaugh A, Baldwin AS, et al. Therapeutically engineered induced neural stem cells are tumour-homing and inhibit progression of glioblastoma. *Nature Communications*. 2016;7:10593

Bago JR, Pegna GJ, Okolie O, Mohiti-Asli M, Lobo EG, Hingtgen SD. Electrospun nanofibrous scaffolds increase the efficacy of stem cell-mediated therapy of surgically resected glioblastoma. *Biomaterials*. 2016;90:116-125

Baker, M. Taking a long, hard look. *Nature* 466, 1137–1138 (2010)

Barry DJ, Durkin CH, Abella JV, Way M. Open source software for quantification of cell migration, protrusions, and fluorescence intensities. *J Cell Biol*. 2015 Apr 13;209(1):163-80. doi: 10.1083/jcb.201501081. Epub 2015 Apr 6. PMID: 25847537; PMCID: PMC4395480

Beltman JB, Marée AF, de Boer RJ. Analysing immune cell migration. *Nat Rev Immunol*. 2009 Nov; 9(11):789-98. doi: 10.1038/nri2638. Epub 2009 Oct 16

Büth H, Luigi Buttigieg P, Ostafe R, Rehders M, Dannenmann SR, Schaschke N, Stark HJ, Boukamp P, Brix. Cathepsin B is essential for regeneration of

scratch-wounded normal human epidermal keratinocytes. *Eur. J. Cell Biol.* 2007;86(11-12):747-61

Cantarella C, Sepe L, Fioretti F, Ferrari MC and Paoletta G. Analysis and modelling of motility of cell populations with MotoCell. *BMC Bioinformatics* 2009, 10 (Suppl 12):S12

Chambers AF, Groom AC, MacDonald IC. Dissemination and growth of cancer cells in metastatic sites. *Nat Rev Cancer.* 2002 Aug;2(8):563-72

Chapnick DA, Jacobsen J, Liu X. The development of a novel high throughput computational tool for studying individual and collective cellular migration. *PLoS ONE.* 2013; 8(12): e82444

Chen S, Bremer AW, Scheideler OJ, Na YS, Todhunter ME, Hsiao S, Bomdica PR, Maharbiz MM, Gartner ZJ, Schaffer DV. Interrogating cellular fate decisions with high-throughput arrays of multiplexed cellular communities. *Nature Communications.* 2016;7:10309

Ciccocioppo R, Cangemi GC, Kruzliak P, Gallia A, Betti E, Badulli C, Martinetti M, Cervio M, Pecci A, Bozzi V, Dionigi P, Visai L, Gurrado A, Alvisi C, Picone C, Monti M, Bernardo ME, Gobbi P, Corazza GR. Ex vivo immunosuppressive effects of mesenchymal stem cells on Crohn's disease mucosal T cells are largely dependent on indoleamine 2,3-dioxygenase activity and cell-cell contact. *Stem Cell Research & Therapy.* 2015;6:137

Codling EA, Plank MJ, Benhamou S. Random walk models in biology. *J R Soc Interface.* 2008 Aug 6;5(25):813-34. doi: 10.1098/rsif.2008.0014

Cordelières FP, Petit V, Kumasaka M, Debeir O, Letort V, Gallagher SJ, Larue L. Automated cell tracking and analysis in phase-contrast videos (iTrack4U): development of Java software based on combined mean-shift processes. *PLoS ONE.* 2013 Nov 27;8(11):e81266. doi: 10.1371/journal.pone.0081266. eCollection 2013

Coutu DL, Schroeder T. Probing cellular processes by long-term live imaging – historic problems and current solutions. *Journal of Cell Science* 2013 126: 3805-3815; doi: 10.1242/jcs.118349

Dai L, Alt W, Schilling K, Retzlik J, Gieselmann V, Magin TM, Kappler J. A fast and robust quantitative time-lapse assay for cell migration. *Experimental Cell Research.* 2005;311(2): 272-280

Dasgupta A, Lim AR, Ghajar CM. 2017. Circulating and disseminated tumor cells: harbingers or initiators of metastasis? *Mol. Oncol.* 11:40–61

De Pascalis C, Etienne-Manneville S. Single and collective cell migration: the mechanics of adhesions. *Mol Biol Cell.* 2017 Jul 7;28(14):1833-1846. doi: 10.1091/mbc.E17-03-0134. PMID: 28684609; PMCID: PMC5541834

Debeir O, Adanja I, Kiss R, Decaestecker C. Models of cancer cell migration and cellular imaging and analysis. In *The Motile Actin System in Health and Disease* (Lambrechts, A. and Ampe, C., eds); 2008. pp. 123–156, Transworld Research Network

Deforet M, Parrini MC, Petitjean L, Biondini M, Buguin A, Camonis J, Silberzan P. Automated velocity mapping of migrating cell populations (AVeMap). *Nat. Methods* 2012 Nov;9(11):1081-3. doi: 10.1038/nmeth.2209. Epub 2012 Oct 14

Dixit R and Cyr R. Cell damage and reactive oxygen species production induced by fluorescence microscopy: effect on mitosis and guidelines for non-invasive fluorescence microscopy. *Plant J.* 2003 Oct;36(2):280-90

Dosch J, Hadley E, Wiese C, Soderberg M, Houwman T, Ding K, Kharazova A, Collins JL, van Knippenberg B, Gregory C, Kofman A. Time-lapse microscopic observation of non-dividing cells in cultured human osteosarcoma MG-63 cell line. *Cell Cycle.* 2018;17(2):174-181. doi: 10.1080/15384101.2017.1395535. Epub 2017 Dec 26. PMID: 29169283; PMCID: PMC5884383

Dufour A, Shinin V, Tajbakhsh S, Guillén-Aghion N, Olivo-Marin JC, Zimmer C. Segmenting and tracking fluorescent cells in dynamic 3-D microscopy with coupled active surfaces. *IEEE Trans Image Process.* 2005 Sep;14(9):1396-410

Dzyubachyk O, van Cappellen WA, Essers J, Niessen WJ, Meijering E. Advanced level-set-based cell tracking in time-lapse fluorescence microscopy. *IEEE Trans Med Imaging.* 2010 Mar;29(3):852-67. doi: 10.1109/TMI.2009.2038693

Faix J and Rottner K. The making of filopodia. *Curr Opin Cell Biol.* 2006 Feb; 18(1):18-25. Epub 2005 Dec 6

Farnum CE, Turgai J, Wilsman NJ. Visualization of living terminal hypertrophic chondrocytes of growth plate cartilage in situ by differential

interference contrast microscopy and time-lapse cinematography. *Journal of Orthopaedic Research: Official Publication of the Orthopaedic Research Society*. 1990;8(5):750-763

Gebäck T, Schulz MM, Koumoutsakos P, Detmar M. TScratch: a novel and simple software tool for automated analysis of monolayer wound healing assays. *Biotechniques*. 2009 Apr;46(4):265-74. doi: 10.2144/000113083

Godley, BF, Shamsi F A, Liang FQ, Jarrett SG, Davies S and Boulton M. Blue light induces mitochondrial DNA damage and free radical production in epithelial cells. *J Biol Chem*.2005 Jun 3;280(22):21061-6. Epub 2005 Mar 29

Grzelak A, Rychlik B and Bartosz G. Light-dependent generation of reactive oxygen species in cell culture media. *Free Radic Biol Med*. 2001 Jun 15;30(12):1418-25

Gupton SL and Gertler FB. Filopodia: the fingers that do the walking. *Sci STKE*.2007 Aug 21;2007(400):re5

Gupton SL, Anderson KL, Kole TP, Fischer RS, Ponti A, Hitchcock-DeGregori SE, Danuser G, Fowler VM, Wirtz D, Hanein D, Waterman-Storer CM. Cell migration without a lamellipodium: translation of actin dynamics into cell movement mediated by tropomyosin. *J Cell Biol*. 2005; 168(4):619–631

Haga RB, Ridley AJ. Rho GTPases: Regulation and roles in cancer cell biology. *Small GTPases*. 2016 Oct;7(4):207-221. Epub 2016 Sep 14

Herman B, Albertini DF. A time lapse video image intensification analysis of cytoplasmic organelle movements during endosome translocation. *The Journal of Cell Biology*. 1984;98(2):565-576

Hirata Y, Li HW, Takahashi K, Ishii H, Sykes M, Fujisaki J. MHC class I expression by donor hematopoietic stem cells is required to prevent NK cell attack in allogeneic, but not syngeneic recipient mice. *PLoS One*. 2015;10(11):e0141785

Horwitz R, Webb D. Cell migration. *Curr Biol*. 2003 Sep 30;13(19):R756-9

Hossain WA, D'Sa C, Morest DK. Interactive roles of fibroblast growth factor 2 and neuro-trophin 3 in the sequence of migration, process outgrowth, and axonal differentiation of mouse cochlear ganglion cells. *Journal of Neuroscience Research*. 2008;86(11):2376-2391

Jain P, Worthylake RA, Alahari SK. Quantitative analysis of random migration of cells using time-lapse video microscopy. *Journal of Visualized Experiments: JoVE*. 2012;63: e3585

Collins JL, van Knippenberg B, Ding K and Kofman AV (November 5th 2018). Time-Lapse Microscopy, Cell Culture, Radwa Ali Mehanna, IntechOpen, doi: 10.5772/intechopen.81199

Jurado C, Haserick JR, and Lee J. Slipping or gripping? Fluorescent speckle microscopy in fish keratocytes reveals two different mechanisms for generating a retrograde flow of actin. *Mol Biol Cell*. 2005; 16(2):507-18

Kam Y, Rejniak KA, Anderson AR. Cellular modeling of cancer invasion: integration of in silico and in vitro approaches. *J Cell Physiol*. 2012 Feb; 227(2):431-8. doi: 10.1002/jcp.22766. PMID: 21465465; PMCID: PMC3687536

Kamlund S, Strand D, Janicke B, Alm K, Oredsson S. Influence of salinomycin treatment on division and movement of individual cancer cells cultured in normoxia or hypoxia evaluated with time-lapse digital holographic microscopy. *Cell Cycle*. 2017;16(21): 2128-2138

Kawakami T, Nabeshima K, Hamasaki M, Iwasaki A, Shirakusa T, Iwasaki H. Small cluster invasion: A possible link between micropapillary pattern and lymph node metastasis in pT1 lung adenocarcinomas. *Virchows Arch*. 2009; 454:61–70. [PubMed: 19002492]

Kron SJ. Digital time-lapse microscopy of yeast cell growth. *Methods in Enzymology*. 2002;351:3-15

Kumar A, Mendoza M. Time-lapse fluorescence microscopy of budding yeast cells. *Methods in Molecular Biology*. 2016;1369:1-8

Kurosaka S, Kashina A. Cell biology of embryonic migration. *Birth Defects Res C Embryo Today*. 2008 Jun;84(2):102-22. doi: 10.1002/bdrc.20125. PMID: 18546335; PMCID: PMC2542983

Lambert AW, Pattabiraman DR, Weinberg RA. Emerging biological principles of metastasis. *Cell*. 2017 Feb 9;168(4):670-691. doi: 10.1016/j.cell.2016.11.037

Lawson CD, Ridley AJ. Rho GTPase signaling complexes in cell migration and invasion *J Cell Biol.* 2018 Feb 5;217(2):447-457. doi: 10.1083/jcb.201612069. Epub 2017 Dec 12

Li K, Miller ED, Chen M, Kanade T, Weiss LE, Campbell PG. Cell population tracking and lineage construction with spatiotemporal context. *Med Image Anal.* 2008 Oct;12(5):546-66. doi: 10.1016/j.media.2008.06.001. Epub 2008 Jun 18

Liang CC, Park AY, Guan JL. In vitro scratch assay: a convenient and inexpensive method for analysis of cell migration in vitro. *Nat Protoc.* 2007;2(2):329-33

Lin HD, Fong CY, Biswas A, Choolani M, Bongso A. Human Wharton's jelly stem cells, its conditioned medium and cell-free lysate inhibit the growth of human lymphoma cells. *Stem Cell Reviews.* 2014;10(4):573-586

Liu, J.S. (2008) Monte Carlo Strategies in Scientific Computing, Springer Science & Business Media

Louvet JN, Carrion C, Stalder T, Alrhoun M, Casellas M, Potier O, Pons MN, Dagot C. Vancomycin sorption on activated sludge Gram+ bacteria rather than on EPS; 3D confocal laser scanning microscopy time-lapse imaging. *Water Research.* 2017 Nov 1;124:290-297. doi: 10.1016/j.watres.2017.07.056. Epub 2017 Jul 26

Macpherson IR, Hooper S, Serrels A, McGarry L, Ozanne BW, Harrington K, Frame MC, Sahai E, Brunton VG. p120-catenin is required for the collective invasion of squamous cell carcinoma cells via a phosphorylation-independent mechanism. *Oncogene.* 2007; 26:5214–5228. [PubMed: 17334396]

Martin P. Wound healing--aiming for perfect skin regeneration. *Science.* 1997 Apr 4;276(5309):75-81

Mayor R, Etienne-Manneville S. The front and rear of collective cell migration. *Nat Rev Mol Cell Biol.* 2016 Feb;17(2):97-109. doi: 10.1038/nrm.2015.14. Epub 2016 Jan 4

Merouane A, Rey-Villamizar N, Lu Y, Liadi I, Romain G, Lu J, Singh H, Cooper LJ, Varadarajan N, Roysam B. Automated profiling of individual cell-cell interactions from high-throughput time-lapse imaging microscopy in

nanowell grids (TIMING). *Bioinformatics*. 2015 Oct 1;31(19):3189-97. doi: 10.1093/bioinformatics/btv355. Epub 2015 Jun 9

Milde F, Franco D, Ferrari A, Kurtcuoglu V, Poulikakos D, Koumoutsakos P. Cell Image Velocimetry (CIV): boosting the automated quantification of cell migration in wound healing assays. *Integr Biol (Camb)*. 2012 Nov;4(11):1437-47. doi: 10.1039/c2ib20113e

Mokhtari Z, Mech F, Zitzmann C, Hasenberg M, Gunzer M, Figge MT. Automated characterization and parameter-free classification of cell tracks based on local migration behavior. *PLoS ONE*. 2013 Dec 6;8(12):e80808. doi: 10.1371/journal.pone.0080808. eCollection 2013

Muller WA. Getting leukocytes to the site of inflammation. *Vet Pathol*. 2013 Jan;50(1):7-22. doi: 10.1177/0300985812469883. PMID: 23345459; PMCID: PMC3628536

Ortega F, Berninger B, Costa MR. Primary culture and live imaging of adult neural stem cells and their progeny. *Methods in Molecular Biology*. 2013;1052:1-11

Penil Cobo M, Libro S, Marechal N, D'Entremont D, Penil Cobo D, Berkmen M. Visualizing bacterial colony morphologies using time-lapse imaging chamber MOCHA. *Journal of Bacteriology*. 2018;200(2):e00413-17

Petitjean L, Reffay M, Grasland-Mongrain E, Poujade M, Ladoux B, Buguin A, Silberzan P. Velocity fields in a collectively migrating epithelium. *Biophys J*. 2010 May 19;98(9):1790-800. doi: 10.1016/j.bpj.2010.01.030

Piltili KM, Cummings BJ, Carta K, Manughian-Peter A, Worne CL, Singh K, Ong D, Maksymyuk Y, Khine M, Anderson AJ. Live-cell time-lapse imaging and single-cell tracking of in vitro cultured neural stem cells - Tools for analyzing dynamics of cell cycle, migration, and lineage selection. *Methods*. 2018 Jan 15;133:81-90. doi: 10.1016/j.ymeth.2017.10.003. Epub 2017 Oct 16

Pulkkinen JO, Elomaa L, Joensuu H, Martikainen P, Servomaa K, Grenman R. Paclitaxel-induced apoptotic changes followed by time-lapse video microscopy in cell lines established from head and neck cancer. *Journal of Cancer Research and Clinical Oncology*. 1996;122(4):214-218

Ranzato E, Martinotti S, Burlando B. Wound healing properties of jojoba liquid wax: an in vitro study. *J Ethnopharmacol.* 2011 Mar 24;134(2):443-9. doi: 10.1016/j.jep.2010.12.042. Epub 2011 Jan 4

Rappel WJ, Edelstein-Keshet L. Mechanisms of Cell Polarization. *Curr Opin Syst Biol.* 2017 Jun;3:43-53. doi: 10.1016/j.coisb.2017.03.005. Epub 2017 Apr 12. PMID: 29038793; PMCID: PMC5640326

Ray N and Acton ST. Active contours for cell tracking. *Proceedings Fifth IEEE Southwest Symposium on Image Analysis and Interpretation, Sante Fe, NM, USA, 2002*, pp. 274-278

Reig G, Pulgar E, Concha ML. Cell migration: from tissue culture to embryos. *Development.* 2014 May;141(10):1999-2013. doi: 10.1242/dev.101451

Ridley AJ. Rho GTPase signalling in cell migration. *Curr Opin Cell Biol.* 2015 Oct;36:103-12. doi: 10.1016/j.ceb.2015.08.005. Epub 2015 Sep 10

Rosello C, Ballet P, Planus E, Tracqui P. Model Driven Quantification of Individual and Collective Cell Migration. *Acta Biotheor.* 2004. 52, 343–363

Sadok A, Marshall CJ. Rho GTPases: masters of cell migration. *Small GTPases.* 2014;5:e29710. doi: 10.4161/sgtp.29710. Epub 2014 Jun 30

Safferling K, Sütterlin T, Westphal K, Ernst C, Breuhahn K, James M, Jäger D, Halama N, Grabe N. Wound healing revised: a novel reepithelialization mechanism revealed by in vitro and in silico models. *J Cell Biol.* 2013 Nov 25;203(4):691-709. doi: 10.1083/jcb.201212020

Sanga S, Frieboes HB, Zheng X, Gatenby R, Bearer EL, Cristini V. Predictive oncology: a review of multidisciplinary, multiscale in silico modeling linking phenotype, morphology and growth. *Neuroimage.* 2007;37 Suppl 1:S120-34. Epub 2007 Jun 7

Schiraldi C, Zappavigna S, D'Agostino A, Porto S, Gaito O, Lusa S, Lamberti M, De Rosa M, De Rosa G, Caraglia M. Nanoparticles for the delivery of zoledronic acid to prostate cancer cells: A comparative analysis through time lapse video-microscopy technique. *Cancer Biology & Therapy.* 2014;15(11):1524-1532

Schmidt GW, Frey O, Rudolf F. TheCellClamper: A convenient microfluidic device for time-lapse imaging of yeast. *Methods in Molecular Biology*. 2018;1672:537-555

Sterckx S, Cockbain J, Pennings G. Patenting medical diagnosis methods in Europe: Stanford University and time-lapse microscopy. *Reproductive Biomedicine Online*. 2017;34(2):166-168

Sterckx S, Cockbain J, Pennings G. Patenting time-lapse microscopy: The European story. *Reproductive Biomedicine Online*. 2014;28(2):146-150

Svensson CM, Medyukhina A, Belyaev I, Al-Zaben N, Figge MT. Untangling cell tracks: Quantifying cell migration by time lapse image data analysis. *Cytometry A*. 2018 Mar;93(3):357-370. doi: 10.1002/cyto.a.23249. Epub 2017 Oct 4

Topman G, Sharabani-Yosef O, Gefen A. A standardized objective method for continuously measuring the kinematics of cultures covering a mechanically damaged site. *Med Eng Phys*. 2012 Mar;34(2):225-32. doi: 10.1016/j.medengphy.2011.07.014. Epub 2011 Aug 5

Trepap X, Chen Z, Jacobson K. Cell migration. *Compr Physiol*. 2012 Oct;2(4):2369-92. doi: 10.1002/cphy.c110012. PMID: 23720251; PMCID: PMC4457291

Turani M, Banfalvi G, Peter A, Kukoricza K, Kiraly G, Talas L, Tanczos B, Dezso B, Nagy G, Kemeny-Beke A. Antibiotics delay in vitro human stem cell regrowth. *Toxicology In Vitro*. 2015 Mar;29(2):370-9. doi: 10.1016/j.tiv.2014.10.013. Epub 2014 Nov 15

Ungphakorn W, Lagerback P, Nielsen EI, Tangden T. Automated time-lapse microscopy a novel method for screening of antibiotic combination effects against multidrug-resistant gram-negative bacteria. *Clinical Microbiology and Infection: The Official Publication of the European Society of Clinical Microbiology and Infectious Diseases*. 2018;24(7):778. e777-778.e714

Ungphakorn W., Malmberg C, Lagerback P, Cars O, Nielsen EI, Tangden T. Evaluation of automated time-lapse microscopy for assessment of in vitro activity of antibiotics. *Journal of Microbiological Methods*. 2017;132:69-75

Urbanek, Simon. (2003). "Rserve – A Fast Way to Provide R Functionality to Applications" in Proc. of the 3rd International Workshop on Distributed

Statistical Computing (DSC 2003), ISSN 1609-395X, Eds.: Kurt Hornik, Friedrich Leisch & Achim Zeileis

Wagner W, Saffrich R, Wirkner U, Eckstein V, Blake J, Ansorge A, Schwager C, Wein F, Miesala K, Ansorge W, D Ho A. Hematopoietic progenitor cells and cellular microenvironment: Behavioral and molecular changes upon interaction. *Stem Cells*. 2005;23(8):1180-1191

Walter MN, Wright KT, Fuller HR, MacNeil S, Johnson WE. Mesenchymal stem cell-conditioned medium accelerates skin wound healing: an in vitro study of fibroblast and keratinocyte scratch assays. *Exp Cell Res*. 2010 Apr 15;316(7):1271-81. doi: 10.1016/j.yexcr.2010.02.026. Epub 2010 Mar 3

Wang PH, Huang BS, Horng HC, Yeh CC, Chen YJ. Wound healing. *J Chin Med Assoc*. 2018 Feb;81(2):94-101. doi: 10.1016/j.jcma.2017.11.002. Epub 2017 Nov 21

Wang W, Goswami S, Sahai E, Wyckoff JB, Segal JE, Condeelis JS. Tumour cells caught in the act of invading: their strategy for enhanced cell motility. *Trends Cell Biol*, 2005 Mar; 15(3):138-45

Wei F, Rong XX, Xie RY, Jia LT, Wang HY, Qin YJ, Chen L, Shen HF, Lin XL, Yang J, Yang S, Hao WC, Chen Y, Xiao SJ, Zhou HR, Lin TY, Chen YS, Sun Y, Yao KT, Xiao D. Cytokine-induced killer cells efficiently kill stem-like cancer cells of nasopharyngeal carcinoma via the NKG2D-ligands recognition. *Oncotarget*. 2015 Oct 27;6(33):35023-39. doi: 10.18632/oncotarget.5280

Weiger MC, Vedham V, Stuelten CH, Shou K, Herrera M, Sato M, Losert W, Parent CA. Real-time motion analysis reveals cell directionality as an indicator of breast cancer progression. *PLoS One*. 2013;8(3):e58859. doi: 10.1371/journal.pone.0058859. Epub 2013 Mar 19

Wells CM, Ridley AJ. Analysis of cell migration using the Dunn chemotaxis chamber and time-lapse microscopy. *Methods in Molecular Biology*. 2005;294:31-41

Wu C. Focal adhesion: a focal point in current cell biology and molecular medicine. *Cell Adh Migr*. 2007 Jan-Mar;1(1):13-8. doi: 10.4161/cam.1.1.4081. Epub 2007 Jan 27. PMID: 19262093; PMCID: PMC2633675

Yang C, Czech L, Gerboth S, Kojima S, Scita G, Svitkina T. Novel roles of forming mDia2 in lamellipodia and filopodia formation in motile cells. PLoS Biol. 2007; 5(11):e317. [PubMed: 18044991]

Yang R, Wang M, Wang J, Huang X, Yang R, Gao WQ. Cell division mode change mediates the regulation of cerebellar granule neurogenesis controlled by the sonic hedgehog signaling. Stem Cell Reports. 2015;5(5):816-828

Yang F, Mackey MA, Ianzini F, Gallardo G, Sonka M. Cell segmentation, tracking, and mitosis detection using temporal context. Med Image Comput Comput Assist Interv. 2005;8(Pt 1):302-9

Web Sites

R - <https://www.r-project.org>

Rserve - <http://rforge.net/Rserve/>

8. LIST OF PUBLICATIONS

Tufano R., Toscano E., Boccia A., Sepe L., Paoletta G. MotoCell, an integrated environment for dynamic analysis of cultured cells movement and proliferation. (manuscript in preparation)

Toscano E., Tufano R., del Giudice G., Sepe L., Paoletta G. A three component model for single cell migration analysis. (manuscript in preparation)